



Generalized mass-conservative finite volume framework for unified saturated–unsaturated subsurface flow

Saumava Dey, Anirban Dhar*

Civil Engineering Department, Indian Institute of Technology Kharagpur, Kharagpur, West Bengal 721302, India



ARTICLE INFO

This manuscript was handled by Corrado Corradi, Editor-in-Chief, with the assistance of Valentina Ciriello, Associate Editor

Keywords:

Subsurface flow
Richards Equation
OpenFOAM®
Stabilized and adaptive time-stepping algorithm
Parallel computation

ABSTRACT

Numerical modeling of saturated–unsaturated flow in porous media is very challenging due to the strong nonlinearity of the Richards Equation in the unsaturated flow zone. Robust and efficient numerical models are essential to simulate the flow dynamics of regional-scale subsurface systems accurately. In this paper, we have presented generalized mass-conservative Finite Volume solvers for pressure head-based and mixed forms of Richards Equation named *subsurfaceFlowFOAM*, developed using OpenFOAM® framework. The solution of Richards Equation often encounters numerical instabilities and convergence issues owing to the inherent nonlinearity of the soil–water characteristic relations and sharp variations in hydrological conditions over time. In this work, we have proposed a stabilized and adaptive time-stepping algorithm that adjusts the time-step size following the solution requirements ensuring smooth convergence. We have further implemented the parallel computation technique through the domain decomposition method to accelerate the computation process for large-scale simulations involved in regional-scale modeling. The numerical results of *subsurfaceFlowFOAM* depict excellent correspondence with the data presented in the literature for a wide variety of subsurface flow problems with deficient cumulative mass balance error. The solution accuracy and the computational efficiency of the solvers ensure their potential applicability to solve multi-dimensional regional-scale subsurface flow problems.

1. Introduction

Water flow in variably saturated porous media is considered among the most complex hydrological flow processes occurring on earth. Following the fundamental laws of hydrodynamics, Richards (1931) established an equation governing the flow of water through partially saturated porous media under the actions of gravity and capillarity. The equation is commonly known as Richards' Equation (RE). However, RE is derived based on the assumption that the non-wetting phase (air) is continuous within the porous media without being trapped in discrete pockets. Hence, air always remains at atmospheric pressure, and RE does not describe its motion within the porous media.

Based on the choice of the dependent variable, we can represent standard RE in three alternative forms, namely, pressure head-based form (h-based), moisture content-based form (θ -based), and mixed-form. Applying any form mentioned above, we can predict water movement only through the unsaturated zone of porous media. Therefore, we cannot use the standard RE for various drainage and irrigation problems encountered in agricultural engineering and groundwater

hydrology that involve the underlying aquifer system. Rubin (1968) took the first initiative toward integrated saturated and unsaturated flow modeling to solve a falling water table experiment in a two-dimensional rectangular soil slab numerically. Nonetheless, Freeze (1971) made a breakthrough attempt by employing a modified form of standard RE for modeling the flow of infiltrated water in the unsaturated zone underneath the ground surface and the confined and unconfined aquifers lying further below.

Unlike aquifer systems, the hydraulic conductivity within the unsaturated layer of porous media is not constant. It varies continuously with the available moisture content, which is again a function of the pressure head. The constitutive relationships among pressure head, moisture content, and hydraulic conductivity in the unsaturated zone are highly nonlinear; thereby, the analytical solution of RE is infeasible except for exceptional cases. The numerical approach is the best possible alternative for solving variably saturated flow problems. Acceptance of any numerical scheme depends on its efficiency at predicting a subsurface system's flow dynamics and its capability to conserve mass in the process. Numerical techniques for solving different forms of RE suffer

* Corresponding author.

E-mail address: anirban@civil.iitkgp.ac.in (A. Dhar).

from various stability and mass conservation issues. The h-based form is the original form of RE derived by Richards (1931) and has been comprehensively used for solving various one-dimensional infiltration and drainage problems (Whisler and Watson, 1968; Freeze, 1969; Haverkamp et al., 1977; Dane and Mathis, 1981; Haverkamp and Vauclin, 1981). With the modification of RE for solving saturated-unsaturated subsurface flow, the modified h-based RE has been extended for modeling both two-dimensional (Cooley, 1971; Neuman, 1973; Cooley, 1983; Huyakorn et al., 1984) and three-dimensional (Freeze, 1971; Huyakorn et al., 1986) flow through porous media. Unfortunately, the numerical approximation of h-based RE incurs significant mass balance error due to high nonlinearity of the specific moisture capacity term (van Genuchten, 1982; Allen and Murphy, 1985; Celia et al., 1990). The numerical formulation of θ -based RE shows better accuracy in mass balance error relative to the h-based form. Considering θ -based RE, the moisture content is not continuous across the water table or the interfaces of soil layers in case of layered heterogeneity. Hence, the applicability of θ -based RE is limited to unsaturated flow problems through uniform soils (Haverkamp et al., 1977; Huyakorn, 2012). The numerical approximation of mixed-form RE overcomes the respective limitations of the h-based and θ -based forms and has been successfully applied for saturated-unsaturated subsurface flow modeling with high global mass balance accuracy (Brutsaert, 1971; Allen and Murphy, 1986; Celia et al., 1990; Clement et al., 1994; Dogan and Motz, 2005; Lai and Ogden, 2015; Li et al., 2021).

In reality, we often come across porous media with layered heterogeneity. We encounter spatial discontinuities among the soil-characteristic parameters in such layered soils, which hinder a smooth numerical solution of RE at the soil interfaces. Multidomain discretization of RE as proposed by Berninger et al. (2015) can be considered a generalized approach for modeling subsurface flow through domains decomposed into non-overlapping layers. Suk and Park (2019) applied a truncated Taylor series expansion to the Kirchhoff head at the material interface to avoid the dyadic characteristics arising in the numerical solution of the Kirchhoff-transformed RE. To model the effect of discontinuity at the intersection of non-overlapping layered soils, Berardi et al. (2020) presented a numerical technique based on mixed MoL-TMoL approach, which satisfactorily handles the solution behavior at the layer interfaces. Kumar et al. (2020) overcame the spatial intricacies experienced in numerical modeling of unsaturated flow through porous media containing fractures by developing an effective RE where they replaced a fracture in the porous media with an interface for RE. Hence, a robust RE solver must ensure a smooth solution at the soil interfaces while numerically modeling variably saturated flow problems in heterogeneous layered porous media.

Researchers have employed a wide range of numerical methods for the development of RE solver, of which Finite Difference (FD) and Finite Element (FE) methods are the most common. FD spatial approximation has been applied for one-dimensional unsaturated flow through vertical soil columns (Day and Luthin, 1956; Whisler and Watson, 1968; Freeze, 1969; Brandt et al., 1971; Haverkamp et al., 1977; Dane and Mathis, 1981; Haverkamp and Vauclin, 1981), and higher-dimensional saturated-unsaturated flow through fractured and porous media (Rubin, 1968; Freeze, 1971; Cooley, 1971; Brutsaert, 1971; Celia et al., 1990; Kirkland et al., 1992; Clement et al., 1994; Dogan and Motz, 2005). An improved version of the FD method — the Integrated Finite Difference (IFD) method has also been used for numerical analysis of fluid flow (Narasimhan and Witherspoon, 1978) as well as simulation of non-isothermal multiphase flow and reactive transport process in permeable media (Finsterle et al., 2008). Researchers have also developed several FE method-based models to solve flow and transport problems in

variably saturated porous media — Galerkin FE method-based models like UNSAT2 (Neuman, 1973), FEMWATER (Yeh and Ward, 1980), SATURN (Huyakorn et al., 1984), FLAMINCO (Huyakorn et al., 1986), ADaptive Hydrology (ADH) (Howington et al., 1999), HYDRUS (Šimunek et al., 2008), and Control Volume FE method-based models like FE Heat and Mass Transfer code (FEHM) (Zyvoloski, 2007), HydroGeoSphere (HGS) (Brunner and Simmons, 2012).

With the advancement of research on subsurface hydrology, scientists have developed generalized computer programs and software packages to model integrated surface-subsurface flow and transport phenomena on regional scales. Kollet and Maxwell (2006) presented a generalized model — ParFlow, coupling the two-dimensional overland flow with an existing three-dimensional FD method-based subsurface flow model (Ashby and Falgout, 1996; Jones and Woodward, 2001). Healy (2008) developed an FD method-based software package (VS2DI) incorporating the flow and heat transport simulator (VS2DH) into the previously developed computer program to simulate solute transport in variably saturated porous media (VS2DT) (Healy, 1990). Trefry and Muffels (2007) developed a Continuous Galerkin FE method-based computer program FEFLOW to simulate density-dependent variably saturated flow and transport, including multi-species reactive transport. To model the process of surface-subsurface flow and their interaction, Camporese et al. (2010) presented the CATCHment HYdrology (CATHY) model, which couples an FE solver for RE with an FD solver for the diffusion wave equation describing the surface flow. We can find another instance of coupling of FE and FD methods in the saturated-unsaturated flow model developed by Gao et al. (2019), where they have used FE and FD methods for spatial discretization in the horizontal and vertical directions, respectively. Yeh et al. (2011) advanced the concept of catchment modeling and developed a watershed-scale numerical model WASH123D that combines solvers for one-dimensional stream or river flow, two-dimensional overland flow, and three-dimensional subsurface flow.

FD and FE schemes lack robustness as they often suffer from numerical instabilities and convergence issues (Freeze, 1971; Celia et al., 1990). Implicit iterative methods like line successive over-relaxation (LSOR) technique or alternating direction implicit (ADI) procedure used in the FD approximation faces convergence difficulties due to time-step limitation introduced by the nonlinearity of the soil-water parameters (Freeze, 1971). However, a fully implicit (backward Euler) time approximation scheme can be a good alternative for FD method-based saturated-unsaturated flow models. In case of problems related to infiltration into parched soil, FE method-based solvers produce oscillatory solutions (Celia et al., 1990). Diagonalisation of the time matrix, inherent to FD approximation, eliminates oscillations from the numerical solution. On the other hand, the mass lumping method is adopted in FE schemes to eliminate oscillations in the numerical solution.

Until recent times, the Finite Volume (FV) method has not been common among researchers for modeling variably saturated subsurface flow. Owing to the functional nonlinearity of involved parameters, RE suffers from mass conservation issues. Since the FV method is highly mass-conservative, it can be a good numerical tool for solving RE. Eymard et al. (1999) pioneered at proving the convergence of the FV scheme for discretization of the elliptic-parabolic RE. Since then, successful attempts have been made in FV method-based modeling of one-dimensional (Lai and Ogden, 2015; Li et al., 2021) and two-dimensional (Manzini and Ferraris, 2004; Aravena and Dussaillant, 2009) infiltration problems. Horgue et al. (2015) developed porousMultiphaseFoam using the open-source FV method-based multiphysics platform OpenFOAM® for modeling three-dimensional multiphase flow through both isotropic

and anisotropic porous media. The *porousMultiphaseFoam* package contains multiphase models for relative permeability and capillarity and also includes a customized Neumann boundary condition to impose phase velocity on the boundaries. Deng and Wang (2017) presented an FV scheme-based saturated–unsaturated flow model using three-dimensional RE in arbitrary coordinates. Consequently, OpenFOAM® based three-dimensional saturated–unsaturated flow models like *suGWFoam* (Liu, 2013) and *RichardsFOAM* (Orgogozo et al., 2014; Orgogozo, 2015) have also been developed.

Another vital aspect involved in the development of a numerical solver for RE is the time discretization technique. The convergence of the iterative linearization process depends mainly on the time-step size considered by the solver. It is necessary to consider small time-steps when the hydrological conditions within the flow domain change very sharply with time. However, small time-steps would unnecessarily increase the overall computation time during smooth variations of hydrological conditions, making the solver inefficient for modeling regional-scale problems. Hence, to restore the efficiency of the numerical scheme, an algorithm should be implemented within the solver, which continuously alters the time-step size based on the evolving hydrological conditions. Researchers have commonly adopted time-stepping algorithms based on the number of iterations required for convergence of the linearization process (Williams and Miller, 1999; Liu, 2013; Orgogozo et al., 2014; Orgogozo, 2015). In some numerical models, a flux-updating algorithm has been implemented where the time-step size is adjusted based on the variations in moisture content occurring due to changes in flux (Kirkland et al., 1992; Lai and Ogden, 2015; Li et al., 2021). Therefore, a suitable adaptive time-stepping algorithm is essential for an efficient RE solver to achieve smooth convergence at minimum computation time.

The parallel computing technique has emerged through which an extensive computation can be broken down into small parts and computed simultaneously through multi-core processors. The application of parallel computing has dramatically curtailed the computation time involved in solving large-scale saturated–unsaturated flow problems (Tracy, 2006; Coumou et al., 2008; Herbst et al., 2008; Maxwell, 2013). We can implement the parallelization strategy in a numerical model, either by domain decomposition or in the form of loop-level parallelism. We can use the loop decomposition approach for a few processors, thereby being a rare option for hydrological modeling. Orgogozo et al. (2014) have used the domain decomposition method for the development of their open-source parallel solver for RE–RichardsFOAM. Hence, the development of parallel solvers is essential for accelerating the simulation of watershed-scale hydrological problems for large time domains.

Owing to the high nonlinearity of RE, its numerical solution is computationally expensive and unreliable at times (Farthing and Ogden, 2017). The focus, thus, should be given to the development of a robust numerical technique that is accurate, mass-conservative, and can be applied to natural soil layers and aquifer systems, subjected to a wide variety of initial and boundary conditions. This paper presents a generalized parallel mathematical model based on FV approximation to evaluate subsurface flow dynamics through heterogeneous porous media. We have developed separate solvers with mass-conservative numerical approximations of both h-based and mixed forms of RE. We have implemented a stabilized and adaptive time-stepping algorithm for smooth convergence and increased computational efficiency. We have also utilized the parallelization framework available in OpenFOAM® for speeding up the process of large-scale simulations. The novelty of the presented work lies in the robustness of the developed RE solvers verified through their performance in reproducing the results of nine

subsurface flow problems that include theoretical examples, laboratory-scale experiments, and field tests. We have also proposed an alternative approach for solving the unsteady-state pumping test in an unconfined aquifer. The proposed methodology considers the actual radius of the pumping well to estimate drawdown in the aquifer, which is independent of grid dimensions. Finally, we have conducted a comparative study of h-based and mixed form solvers and have commented on their respective efficacies through the solved test examples.

2. Governing equations

In conjunction with Darcy's law, the law of conservation of mass leads to the derivation of RE governing the flow of water in unsaturated porous media. The movement of water in porous media primarily takes place due to gravity and variations in the pressure head. However, the flow of water through the unsaturated zone is sometimes governed by the change in density of water occurring due to temperature fluctuations or alterations in solute concentration. In this study, we have neglected the effects of changes in temperature and solute concentration and have considered the density of water to remain constant throughout the flow process. We have used the modified RE presented by Freeze (1971), introducing the specific storage term, to use a single equation describing the flow of water through both saturated and unsaturated zones of the subsurface. We can present the modified RE as the following:

- **h-based form:**

$$\left[S_s \frac{\theta}{\eta} + C_w(h) \right] \frac{\partial h(\mathbf{x}, t)}{\partial t} = \nabla \cdot [\mathbf{K}(h) \nabla (h(\mathbf{x}, t) + z)] + q_s \quad (1)$$

- **Mixed form:**

$$\frac{\partial \theta}{\partial t} + S_s \frac{\theta}{\eta} \frac{\partial h(\mathbf{x}, t)}{\partial t} = \nabla \cdot [\mathbf{K}(h) \nabla (h(\mathbf{x}, t) + z)] + q_s \quad (2)$$

$$\mathbf{x} \in \Omega$$

$$t \in [0, T_f]$$

We can express specific storage S_s with the compressibility terms, α and β as:

$$S_s = \gamma_{\text{water}} [\alpha + \eta \beta] \quad (3)$$

3. Soil–water characteristic model

Within the unsaturated zone, moisture content θ , hydraulic conductivity \mathbf{K} and specific moisture capacity C_w are nonlinear functions of the pressure head h . Scientists have formulated several empirical models for representing the soil–water relationship in the unsaturated zone. Some of these models are — Brooks and Corey model (Brooks and Corey, 1964), Brooks–Corey–Burdine model (Brooks and Corey, 1966), van Genuchten–Mualem model (van Genuchten, 1980), van Genuchten and Nielsen model (van Genuchten and Nielsen, 1985), and general power formula (Dogan, 1999). In this work, we have adopted the van Genuchten–Mualem model as it is prevalent and has been widely accepted by researchers. The constitutive relationship of pressure head and soil–water parameters as presented in the van Genuchten–Mualem model are as the following:

- **Moisture content $[\theta]$:**

$$\theta = \begin{cases} \theta_r + S_e(h)(\theta_s - \theta_r) & h < 0 \\ \theta_s & h \geq 0 \end{cases} \quad (4)$$

where,

$$S_e(h) = \left[1 + \left| \alpha_w h \right|^{\beta_w} \right]^{-\gamma_w} \quad (5)$$

$$\gamma_w = 1 - \frac{1}{\beta_w}$$

- **Hydraulic conductivity $[K]$:**

$$K(h) = \begin{cases} K_s S_e(h)^{\frac{1}{\beta_w}} \left[1 - \left(1 - S_e(h)^{\frac{1}{\beta_w}} \right)^{\gamma_w} \right]^2 & h < 0 \\ K_s & h \geq 0 \end{cases} \quad (6)$$

- **Specific moisture capacity $[C_w]$:**

$$C_w(h) = \frac{\partial \theta}{\partial h} = \begin{cases} \frac{\alpha_w \gamma_w (\theta_s - \theta_r)}{(1 - \gamma_w)} S_e(h)^{\frac{1}{\beta_w}} \left[1 - S_e(h)^{\frac{1}{\beta_w}} \right]^{\gamma_w} & h < 0 \\ 0 & h \geq 0 \end{cases} \quad (7)$$

4. Development of *subsurfaceFlowFOAM*

subsurfaceFlowFOAM is a three-dimensional FV method-based model for evaluating the pressure head distribution in the subsurface flow domain. In this project, we have adopted the FV method for the numerical approximation of RE as it is inherently mass-conservative, and we can apply it to geometrically complex domains overlaid by a regular-structured or unstructured grid system (Dey and Dhar, 2020). For the development of *subsurfaceFlowFOAM*, we have used the framework of FV-based computational fluid dynamics toolbox OpenFOAM® (Jasak, 1996). Working in OpenFOAM® has helped us to develop our numerical model on a globally acclaimed open-source platform using the functions and differential operators from the toolbox library. One of the most significant advantages of developing solvers in the OpenFOAM® platform is that it facilitates parallel computing. The parallel computing technique is implemented in OpenFOAM® framework through the process of domain decomposition employing the communication protocols of Message Passing Interface (MPI). *RichardsFOAM*, which is an existing RE solver developed on OpenFOAM® platform, is not robust and experiences certain runtime limitations. *RichardsFOAM* employs the h-based form of modified RE with the standard chord slope (SCS) approximation for the specific moisture capacity term C_w . The *RichardsFOAM* solver fails when specific storage S_s is absent (strictly unsaturated flow problems) or has a value of zero. Moreover, *RichardsFOAM* has been developed for solving variably saturated flow problems through isotropic porous media. To guarantee the robustness of a solver, we need to overcome the limitations suffered by *RichardsFOAM*. In *subsurfaceFlowFOAM* we have modified the h-based RE solver of *RichardsFOAM* by introducing a switching algorithm for initializing the specific moisture capacity term C_w . We have also developed a mixed form-based RE solver in *subsurfaceFlowFOAM* following the modified Picard iteration scheme (Celia et al., 1990).

4.1. Approximation of the specific moisture capacity term C_w

Researches in unsaturated zone hydrology claim that the mixed-form RE guarantees better mass conservation than the h-based form. The trick at achieving perfect mass balance for RE lies in the numerical approximation and representation of the specific moisture capacity term (Kosugi, 2008). In the numerical modeling of RE using the h-based form, we incur significant mass balance error when we use the traditional analytical derivative form of C_w given in Eq. (7). The mass imbalance occurs because the specific moisture capacity function is highly nonlinear and varies significantly from the FD-based approximated form at discrete levels. Celia et al. (1990) proposed a mass-conservative approach for the numerical approximation of the mixed-form RE known as the modified Picard iteration scheme. In their approach, they have expanded the unknown moisture content using Taylor series expansion. With the superscripts m denoting the Picard iteration level and n denoting the time-level, we can express the expanded form of the unknown moisture content $\theta^{m+1,n+1}$ as the following:

$$\begin{aligned} \theta^{m+1,n+1} &= \theta^{m,n+1} + \left(\frac{\partial \theta}{\partial h} \right)^{m,n+1} \Delta h + O\left(\Delta h^2 \right) \\ \theta^{m+1,n+1} &\cong \theta^{m,n+1} + C_w(h)^{m,n+1} \Delta h \end{aligned} \quad (8)$$

where,

$$\Delta h = h^{m+1,n+1} - h^{m,n+1}$$

Applying Eq. (8), we can expand the time derivative of moisture content θ as the following:

$$\frac{\partial \theta}{\partial t} \cong \frac{\theta^{m,n+1} - \theta^n}{\Delta t} + C_w(h)^{m,n+1} \left(\frac{h^{m+1,n+1} - h^{m,n+1}}{\Delta t} \right) \quad (9)$$

Rathfelder and Abriola (1994) presented a mass-conservative approach for numerically approximating the h-based RE applying standard chord slope (SCS) approximation scheme for discretizing the specific moisture capacity term C_w . They have also proved that their approach becomes numerically equivalent to the modified Picard iteration scheme, thereby ensuring mass conservation. We can approximate the specific moisture capacity term C_w applying the SCS scheme like the following:

$$C_w = \frac{\partial \theta}{\partial h} = \frac{\theta^{m,n+1} - \theta^n}{h^{m,n+1} - h^n} \quad (10)$$

In *subsurfaceFlowFOAM*, we have developed solvers based on both h-based and mixed forms of RE. The mixed form solver implements the modified Picard iteration scheme, whereas the h-based solver adopts the SCS scheme to approximate specific moisture capacity term C_w . With the SCS approximation scheme, the initialization of C_w requires special attention. In general, we begin the iterative process by setting the values of $\theta^{m,n+1}$ and θ^n to the initial θ values for the entire domain. The initial approximation of C_w becomes zero when evaluated using the Eq. (10). In the absence of specific storage S_s , the time derivative on the left-hand side of the Eq. (1) becomes non-existent, thereby forcing a steady-state solution after the first time-step. *RichardsFOAM* lacks the robustness expected from the solver due to this limitation. To address this issue, we have proposed an algorithm where we have initialized C_w with the traditional analytical derivative form whenever specific storage S_s is zero (Algorithm 1). In the subsequent iterations, however, we have approximated C_w using the SCS scheme. Through this approach, the mass balance error increases during the early time steps and later goes down as the solution progresses with time.

Algorithm 1: C_w initialization algorithm

Input: Richards Equation form, C_w approximation form
Output: C_w

1 if *Richards Equation form = h-based* then
2 if *C_w approximation form = Analytical derivative* then
3 C_w computed using Equation (7)
4 else if *C_w approximation form = SCS* then
5 if $S_s \approx 0$ then
6 C_w computed using Equation (7)
7 else
8 C_w computed using Equation (10)
9 else if *Richards Equation form = mixed* then
10 C_w computed using Equation (7)

4.2. Linearization technique

Due to nonlinear dependence of the soil–water parameters $[\theta, \mathbf{K}, C_w]$ on the pressure head h , RE is one of the most complex equations to solve directly. Hence, we need to adopt an iterative linearization procedure to obtain the numerical solution. Some of the iterative methods commonly used for solving RE are — Newton’s method and Picard iteration method. In *subsurfaceFlowFOAM*, we have adopted the Picard iteration method for linearizing both the h-based and mixed forms of RE given in the Eqs. (1) and (2) respectively. Applying Eq. (9), we can write the linearized mixed form of RE as the following:

$$\frac{\theta^{m,n+1} - \theta^n}{\Delta t^{n+1}} + C_w(h)^{m,n+1} \left(\frac{h^{m+1,n+1} - h^{m,n+1}}{\Delta t^{n+1}} \right) + S_s \frac{\theta^{m,n+1}}{\eta} \frac{h^{m+1,n+1} - h^n}{\Delta t^{n+1}} \\ = \nabla \cdot \left[\mathbf{K}(h)^{m,n+1} \nabla \left(h^{m+1,n+1} + z \right) \right] + q_s^{n+1} \quad (11)$$

Rearranging the terms of Eq. (11), we can rewrite it as the following:

$$\left(C_w(h)^{m,n+1} + S_s \frac{\theta^{m,n+1}}{\eta} \right) \left[\frac{h^{m+1,n+1} - h^{m,n+1}}{\Delta t^{n+1}} \right] \\ = \nabla \cdot \left[\mathbf{K}(h)^{m,n+1} \nabla \left(h^{m+1,n+1} + z \right) \right] + q_s^{n+1} - \frac{\theta^{m,n+1} - \theta^n}{\Delta t^{n+1}} - S_s \frac{\theta^{m,n+1}}{\eta} \left[\frac{h^{m,n+1} - h^n}{\Delta t^{n+1}} \right] \quad (12)$$

Implementing the SCS scheme for approximating the specific moisture capacity term C_w , we can present the linearized h-based form of RE as the following:

$$\left(S_s \frac{\theta^{m,n+1}}{\eta} + \frac{\theta^{m,n+1} - \theta^n}{h^{m,n+1} - h^n} \right) \frac{h^{m+1,n+1} - h^n}{\Delta t^{n+1}} \\ = \nabla \cdot \left[\mathbf{K}(h)^{m,n+1} \nabla \left(h^{m+1,n+1} + z \right) \right] + q_s^{n+1} \quad (13)$$

We have solved the set of linear algebraic equations given in the Eqs.

(12) and (13) using the Pre-conditioned Conjugate Gradient (PCG) solver with a Diagonal Incomplete Cholesky (DIC) preconditioner. The above solver has advantages over other iterative matrix solvers by being computationally inexpensive and showing faster convergence (Celia et al., 1990; Clement et al., 1994; Dogan, 1999).

4.3. Stabilized and adaptive time-stepping algorithm

In *subsurfaceFlowFOAM*, we have implemented a stabilized and adaptive time-stepping strategy based on ‘Empirically BASeD Time Step’ (EBATS) scheme (Williams and Miller, 1999) not only to facilitate smooth convergence but also to reduce the computation time and expenses. If the *subsurfaceFlowFOAM* solvers require more than N_{P_u} iterations to converge, or if the solvers fail to converge even after $N_{P_{max}}$ iterations, the algorithm decreases the time-step size by the factor δ_f to ensure smooth convergence. On the other hand, if the solvers converge within N_{P_l} iterations successively for $N_{ST_{max}}$ time-steps, the algorithm increases the time-step size for the next time-level by a factor δ_f . Moreover, the algorithm bounds the time-step size within the prescribed lower and upper limits of Δt_{min} and Δt_{max} respectively. The stabilization technique introduced in this time-stepping algorithm examines the convergence stability of the solver at the current Δt before increasing the time-step size. Hence, if we start the simulation process with a small time-step size, the chances of convergence failure get reduced. A major drawback in the time-stepping algorithm adopted in *RichardsFOAM* is that whenever convergence fails, the algorithm decreases the time-step size and proceeds to the next time level without recomputing the solution for the current time level. In case of convergence failure at a time-level n in *subsurfaceFlowFOAM*, the algorithm recomputes the solution for time level n with a reduced time-step size. Thus, the time-stepping algorithm adopted in *subsurfaceFlowFOAM* (Algorithm 2) is flexible at adapting to the convergence requirements of the solvers, which ensures smooth convergence for all time-steps, consistently preserving the mass balance in the system.

Algorithm 2: Stabilized and adaptive time-stepping algorithm

Input: $N_P, s_c, \Delta t^n, N_{P_l}, N_{P_u}, N_{P_{max}}, N_{ST_{max}}, \Delta t_{min}, \Delta t_{max}, \delta_f$
Output: Δt^{n+1}

```

1 if ( $N_P > N_{P_u}$ ) then
2   if ( $N_{P_u} < N_P < N_{P_{max}}$ ) then
3      $\Delta t^{n+1} \leftarrow \max\left(\frac{\Delta t^n}{\delta_f}, \Delta t_{min}\right)$ 
4      $s_c \leftarrow 0$ 
5   else if ( $N_P = N_{P_{max}}$ ) then
6      $\Delta t^n \leftarrow \max\left(\frac{\Delta t^n}{\delta_f}, \Delta t_{min}\right)$ 
7      $s_c \leftarrow 0$ 
8   else
9     Restart simulation from the previous time-level  $t^n$ .
10  else if ( $N_{P_l} < N_P < N_{P_u}$ ) then
11     $\Delta t^{n+1} \leftarrow \Delta t^n$ 
12     $s_c \leftarrow 0$ 
13  else
14    if ( $N_P < N_{P_l}$ ) and ( $s_c < N_{ST_{max}}$ ) then
15       $\Delta t^{n+1} \leftarrow \Delta t^n$ 
16       $s_c \leftarrow s_c + 1$ 
17    else if ( $N_P < N_{P_l}$ ) and ( $s_c = N_{ST_{max}}$ ) then
18       $\Delta t^{n+1} \leftarrow \min(\delta_f \Delta t^n, \Delta t_{max})$ 
       $s_c \leftarrow 0$ 

```

In this paper, we have considered the values of $N_{P_l} = 3$, $N_{P_u} = 95$, $N_{P_{max}} = 100$, $N_{ST_{max}} = 10$, $\delta_f = 1.25$, and $\Delta t_{min} = \Delta t_0$ for the numerical test cases.

4.4. Convergence criteria

Like accuracy, another vital aspect of iterative methods for solving nonlinear equations is the required computational effort. Careful selection of a convergence criterion optimizes the incurred computational expenses by reducing the number of iterations the solver needs to converge. Huang et al. (1996) have mentioned three convergence criteria that we can implement on Picard iteration schemes adopted for the numerical solution of the h-based and mixed forms of RE.

- **Standard pressure head criterion:**

$$|h^{m+1,n+1} - h^{m,n+1}| \leq \delta_{h_{tol}} \quad (14)$$

- **Mixed pressure head criterion:**

$$|h^{m+1,n+1} - h^{m,n+1}| \leq \delta_{h_{retol}} |h^{m+1,n+1}| + \delta_{h_{tol}} \quad (15)$$

- **Standard moisture content criterion:**

$$|\theta^{m+1,n+1} - \theta^{m,n+1}| \leq \delta_{\theta_{tol}} \quad (16)$$

In this paper, we have adopted the standard moisture content criterion with a tolerance of $\delta_{\theta_{tol}} = 10^{-6}$ for the numerical test cases because of its proven efficiency in terms of both accuracy and acquired computational burden.

4.5. Mass balance error

Mass balance accuracy is an essential criterion for the efficiency of a

numerical model adopted for hydrological modeling. In saturated-unsaturated flow modeling, mass conservation is dependent not only on the adopted numerical approximation scheme but also on the form of RE selected for the flow model. Mass balance error (MBE) measures the ability of a model to conserve global mass within the domain of interest. Ideally, the change of mass of water within the domain should equal the mass of water entering or leaving the domain through its boundaries during a specific time interval. An error occurs when the masses mentioned above are not equal, and we define the error as mass balance error. We can calculate the percentage of cumulative MBE within the domain at a given time as the following:

$$MBE(t^{n+1}) = \left| 1 - \frac{\sum_{i=1}^{N_{ele}} \left[(\theta_i^{n+1} - \theta_i^0) + S_s \frac{\theta^{n+1}}{\eta} (h_i^{n+1} - h_i^0) \right] V_i}{\sum_{k=1}^{n+1} \sum_{j=1}^{N_{Bf}} F_{\phi} |j|^k \Delta t^k} \right| \times 100\% \quad (17)$$

Although mass conservation does not guarantee the accuracy of a numerical solution, a cumulative MBE of less than 1% at the end of the total simulation period is desirable for the potential acceptance of a numerical model (Rathfelder and Abriola, 1994).

5. Numerical tests

To demonstrate the applicability of *subsurfaceFlowFOAM*, we have performed a wide variety of one-dimensional, two-dimensional, and three-dimensional tests, including some benchmark problems, laboratory tests, and field-scale tests. We have developed some custom boundary conditions in OpenFOAM® as required for solving some of the test case problems. We have presented an elaborate description of these custom boundary conditions and the boundary conditions used from OpenFOAM® library while demonstrating the respective test case problems.

5.1. TC1: Simple one-dimensional infiltration test

This simple one-dimensional infiltration test is a benchmark problem

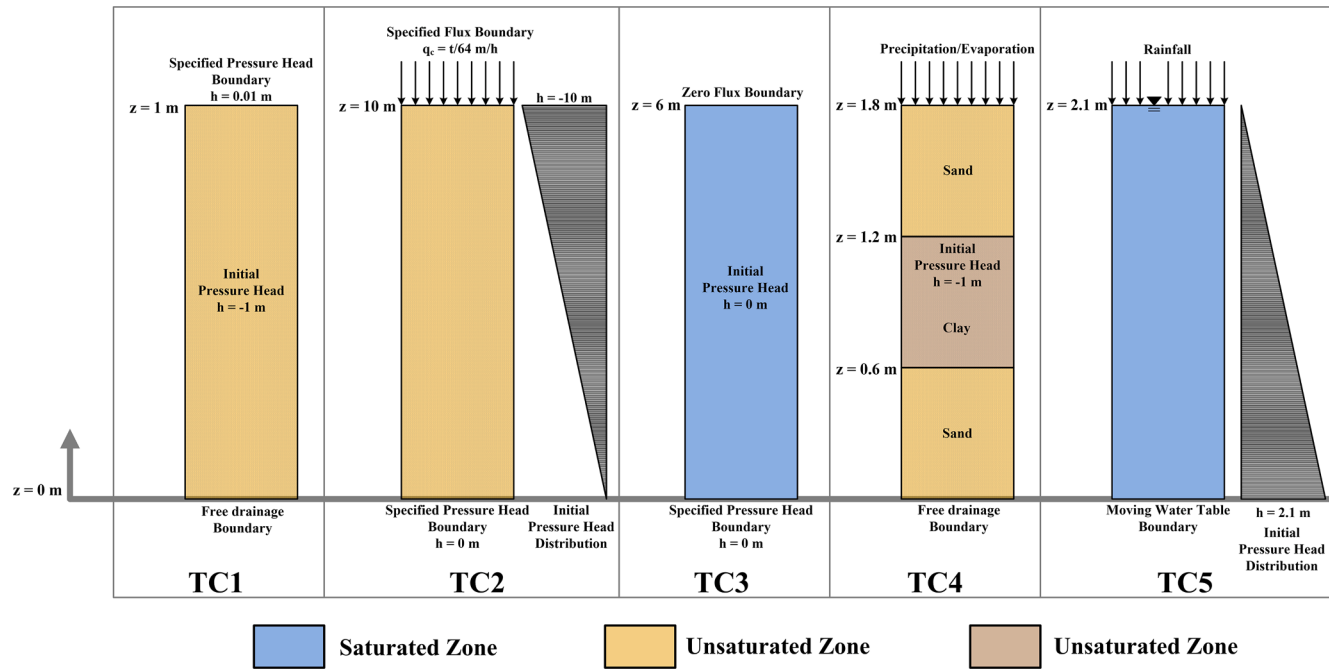


Fig. 1. Schematic diagram of the domain alongside the initial and boundary conditions considered for TC1, TC2, TC3, TC4 & TC5.

that has been used for the validation of *RichardsFOAM* (Orgogozo et al., 2014) in transient conditions. The test domain is a 1 m long homogeneous loamy soil column. The top boundary acts as a specified pressure head boundary, whereas free drainage occurs from the bottom of the soil column (Fig. 1).

- **Specified pressure head boundary:** We have specified the pressure head on a domain boundary by the following function:

$$h(\mathbf{x}, t) = h_c(\mathbf{x}, t) \quad (18)$$

We have prescribed specified pressure head boundary in *subsurfaceFlowFOAM* using *fixedValue* type boundary condition from OpenFOAM® library.

- **Free-drainage boundary:** We have described the free-drainage condition on a domain boundary by the following gradient function:

$$-[\mathbf{K}(h) \nabla h(\mathbf{x}, t)] \cdot \hat{\mathbf{n}} = 0 \quad (19)$$

We have specified free-drainage condition in *subsurfaceFlowFOAM* using *fixedGradient* type boundary condition from OpenFOAM® library with the gradient value equal to zero.

We have discretized the soil column into 100 regular elements, each

size 0.01 m. We have considered the soil column initially unsaturated with a uniform pressure head of -1 m throughout its length. The specified pressure head on the top boundary is 0.01 m . We have listed the soil parameters in Table 1. Considering $\Delta t_0 = 1\text{ s}$ and $\Delta t_{max} = 3600\text{ s}$, we have run the simulation for 24 h using both h-based and mixed-form RE solvers.

5.2. TC2: One-dimensional infiltration and redistribution test

Paniconi et al. (1991) presented a one-dimensional infiltration and redistribution problem to compare the performance of six different time discretization strategies for solving the unmodified RE. Just like SU3D model (Dogan and Motz, 2005) and *suGWFoam* (Liu, 2013), we have used this example as one of the test cases for the validation of *subsurfaceFlowFOAM*. The test case involves a 10 m long homogeneous soil column whose top and bottom boundaries are subjected to specified time-varying flux and specified pressure head, respectively (Fig. 1).

- **Specified flux boundary:** We have specified the flux at a domain boundary by the following function:

$$-[\mathbf{K}(h) \nabla (h(\mathbf{x}, t) + z)] \cdot \hat{\mathbf{n}} = q_c(\mathbf{x}, t) \quad (20)$$

In *subsurfaceFlowFOAM*, we have developed

Table 1
List of soil parameters.

Parameter	TC1	TC2	TC3	TC5	TC6	TC8
$K_s(\text{m/d})$	0.25	120	0.25	17.52	8.4	50
$S_s(\text{m}^{-1})$	10^{-5}	10^{-3}	0	0	0	0
θ_s	0.43	0.45	0.33	0.381	0.3	0.45
θ_r	0.078	0.08	0	0.02	0.01	0.1
ϵ	0.43	0.45	0.33	0.381	0.3	0.45
$\alpha_w(\text{m}^{-1})$	3.6	-0.33	1.43	2.5	3.3	1.65
β_w	1.56	3.0	1.506	9.0	4.1	2.0

Table 2

List of soil parameters for TC4 and TC7.

Parameter	Sand	Clay
K_s (m/d)	5.41	0.13
S_s (m ⁻¹)	10^{-5}	10^{-5}
θ_s	0.366	0.469
θ_r	0.029	0.106
ϵ	0.366	0.469
α_w (m ⁻¹)	2.80	1.04
β_w	2.239	1.395

specifiedConstantFluxBC type boundary condition for specifying time-invariant flux condition on the domain boundary. To specify time-varying flux on a boundary, we have developed problem-specific flux boundary conditions namely, specifiedTransientFluxBC1 and specifiedTransientFluxBC2.

Assuming a grid size of 0.01 m, we have discretized the soil column into 1000 regular elements. We have considered the initial pressure head distribution within the soil column to be hydrostatic with zero pressure head at the bottom boundary. To specify the time-varying flux at the top boundary, we have used specifiedTransientFluxBC1 type boundary condition where the flux function q_c is given by:

$$q_c = \frac{t}{64} \text{ m/h} \quad (21)$$

We have listed the soil parameters considered by Paniconi et al. (1991) in Table 1. We have conducted the simulation for 32 h using $\Delta t_0 = 1$ s and $\Delta t_{max} = 20$ s.

5.3. TC3: Free-drainage test

In this test case, we have carried out numerical modeling of the free-drainage experiment conducted at the Los Alamos National Laboratory using a 6 m deep lysimeter (Abeele, 1984; Forsyth et al., 1995) (Fig. 1). We have selected this example because it demonstrates the transition from saturated to unsaturated conditions due to free drainage from the bottom of the soil column. To ensure that no water enters the soil column, we have imposed zero flux on the top boundary using specifiedConstantFluxBC type boundary condition with $q_c = 0$. At the bottom boundary, we have maintained a zero pressure head so that water drains off continuously. We have discretized the soil column into 600 regular

elements and have initialized each element with zero pressure head to establish saturated conditions within the soil column. We have presented the soil parameters considered in this study in Table 1. Then, we have considered the adaptive time-step parameters, $\Delta t_0 = 0.1$ s and $\Delta t_{max} = 3600$ s to run the simulation for 100 days.

5.4. TC4: Infiltration test through a heterogeneous column with time-varying Boundary Condition

We have chosen the example presented in Li et al. (2021) to demonstrate the effectiveness of subsurfaceFlowFOAM in modeling subsurface flow through a soil column with layered heterogeneity. The soil column is 1.8 m long with a clay layer bounded by sand layers on the top and bottom, as shown in Fig. 1. The specific properties of sand and clay are summarized in Table 2. The top boundary of the soil column acts as a time-varying specified flux boundary, whereas free drainage occurs from the bottom. The time-varying flux is the daily infiltration/evaporation data for the simulation period of 20 days, as displayed in Fig. 2. In subsurfaceFlowFOAM, to specify time-varying flux on a domain boundary where q_c is presented in the form of time-series data, we have developed the boundary condition type specifiedTransientFluxBC2. We have discretized the soil column into 360 regular elements and have initialized each element with a pressure head of -1 m. We have performed the flow simulation through the soil column for 20 days assuming $\Delta t_0 = 1$ s and $\Delta t_{max} = 20$ s.

5.5. TC5: Laboratory infiltration experiment with falling water table

In this example, we have attempted to numerically model the laboratory infiltration experiment with a falling water table conducted by Childs and Poulovassilis (1962). We have computed the steady-state moisture content profile above the water table falling at a constant velocity with the top boundary subjected to constant rainfall intensity. Lai and Ogden (2015) have also used this example for the validation of their proposed numerical model. They have derived the van Genuchten–Mualem soil–water characteristic parameters from the moisture characteristic curve given in Childs and Poulovassilis (1962). We have considered these calibrated soil parameters for our simulation as listed in Table 1.

- **Moving water table boundary:** In the case of a moving water table, the pressure head at the bottom boundary varies with time as a function of the velocity of the moving water table. We have specified the pressure head at the bottom boundary by the following function:

$$h(\mathbf{x}, t) = z_{wt} + v_z t \quad (22)$$

We have assumed the velocity v_z to be positive when the water table rises and vice versa. We have developed the boundary condition type movingWaterTableBC in subsurfaceFlowFOAM to specify the pressure head at the bottom boundary in case of moving water table.

The sand column considered in this study is 1.5 m long Fig. 1. We have discretized the sand column into 300 regular elements, each size 0.005 m. We have assumed the water table to be located at the top boundary at $t = 0$ s. Initially, the sand column is wholly saturated with the hydrostatic distribution of the pressure head. Assuming different water table fall velocities and rainfall intensities, we have carried out seven simulations with:

1. $v_z = 0.172$ m/h and $q_c = 0.0265, 0.06$ & 0.1 m/h
2. $v_z = 0.344$ m/h and $q_c = 0.0265, 0.06, 0.1$ & 0.2 m/h

We have run the simulations assuming $\Delta t_0 = 1$ s and $\Delta t_{max} = 20$ s, until the falling water table reaches the bottom of the sand column and we achieve a steady moisture content profile within the column.

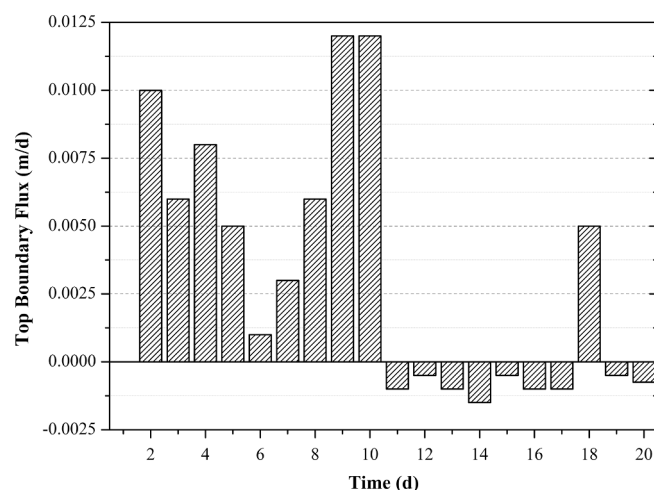


Fig. 2. Time-varying flux on the top boundary of the soil column considered in TC4.

5.6. TC6: Two-dimensional variably saturated water table recharge test

We have validated the applicability of *subsurfaceFlowFOAM* for two-dimensional problems by modeling the transient, two-dimensional saturated-unsaturated water table recharge experiment conducted by [Vauclin et al. \(1979\)](#), [Clement et al. \(1994\)](#), [Dogan and Motz \(2005\)](#) and [Liu \(2013\)](#) have previously considered this benchmark problem to validate their respective numerical models. The flow domain in this example is a rectangular soil slab of length 6 m and depth 2 m. We have tabulated the soil parameters used by [Vauclin et al. \(1979\)](#) in their experiment in [Table 1](#). Initially, the water table is at the height of 0.65 m from the bottom of the domain. A constant flux of 0.14791 m/s is applied at the soil surface throughout 1 m at the center of the top boundary. The remaining span of the top surface was kept covered to restrict evaporation losses during the experiment, and we have treated it as a no-flow boundary during simulation. The bottom of the domain is impervious, and no flow occurs through it. The left and the right boundaries below the water table are specified pressure head boundaries where the pressure head distribution is hydrostatic. However, no flow occurs through the left and the right boundaries above the water table. [Fig. 3](#) shows a schematic diagram representing the domain geometry alongside the initial and boundary conditions considered for the test example.

- **Hydrostatic pressure head boundary:** We have specified hydrostatic distribution of pressure head on a boundary by the following function:

$$h(\mathbf{x}, t) = z_{wt} - z \quad (23)$$

In *subsurfaceFlowFOAM*, we have developed the boundary condition type *hydrostaticBC* to impose hydrostatic pressure head distribution on a domain boundary.

We have discretized the study domain into 2400 rectangular elements with $\Delta x = 0.1 \text{ m}$ and $\Delta z = 0.05 \text{ m}$. We have assumed the initial distribution of pressure head to be hydrostatic throughout the domain. Considering $\Delta t_0 = 1 \text{ s}$ and $\Delta t_{max} = 360 \text{ s}$, we have modeled the flow in the domain for 8 h.

5.7. TC7: Two-dimensional perched water table test

In this example, we have simulated the problem of developing a

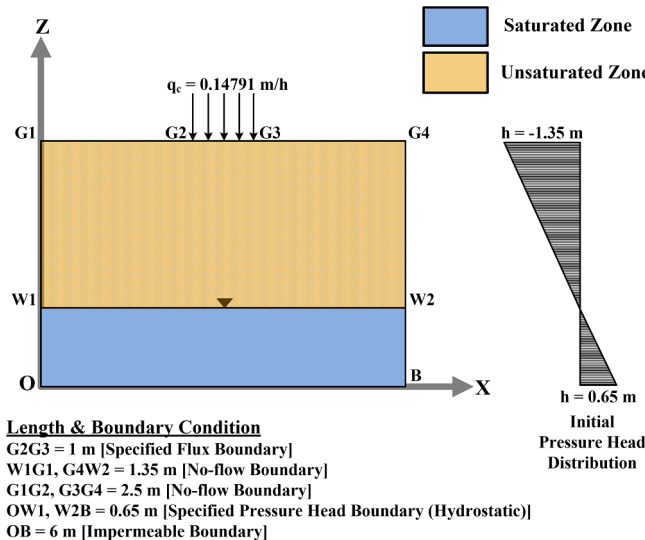


Fig. 3. Schematic diagram of the rectangular flow domain alongside the initial and boundary conditions considered for TC6.

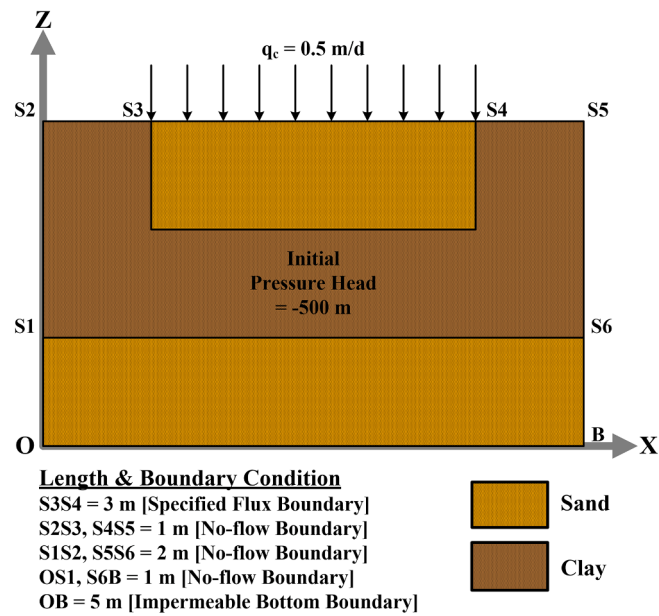


Fig. 4. Schematic diagram of the rectangular flow domain alongside the initial and boundary conditions considered for TC7.

perched water table surrounded by arid unsaturated conditions ([Kirkland et al., 1992](#)). The flow domain is a 5 m long and 3 m deep layered rectangular soil slab whose all boundaries are closed except where infiltration occurs at a rate of 0.5 m/d ([Fig. 4](#)). For developing a perched water table, sand is bounded by a 1 m thick clay barrier of very low permeability on the left, right, and bottom. The properties of sand and clay are the same as considered for TC4, given in [Table 2](#). As the effects of compressibility of the porous medium were neglected by [Kirkland et al. \(1992\)](#), we have considered the specific storage to be zero for this example. We have discretized the domain into an unstructured grid system with 21970 prismatic elements. In order to replicate initial arid conditions within the soil layers, we have considered an initial pressure head of -500 m within the domain. We have run the simulation for 24 h with $\Delta t_0 = 0.01 \text{ s}$ and $\Delta t_{max} = 20 \text{ s}$ to examine the formation of a perched water table above the clay layer.

5.8. TC8: Three-dimensional water table recharge test in response to rainfall

To extend the applicability of *subsurfaceFlowFOAM* to three-dimensional problems, we have utilized the water table recharge test in an unconfined aquifer presented by [Beegum et al. \(2018\)](#). As shown in [Fig. 5](#), the hypothetical domain is 4000 m long, 8000 m broad, and 15 m deep with a bed slope of 0.001 along its length. The flow domain is homogeneous with the soil parameters listed in [Table 1](#). An impermeable boundary bounds the bottom of the unconfined aquifer. On the left and right boundaries, the water table is maintained at the height of 7 m and 0.9 m from the bottom, respectively. Hence, hydrostatic distribution of pressure head is maintained along these boundaries below the water table. However, we have specified a constant pressure head of -1.25 m on the left and right boundaries above the water table. Boundaries on the front and the back along the length of the domain are no-flow boundaries. Initially, we have considered hydrostatic distribution of pressure head within the domain with the water table varying linearly between the heights maintained on the left and the right boundaries. The monthly precipitation data is specified as the time-varying flux on the top boundary, as presented in [Fig. 5](#). We have discretized the domain into a structured-regular grid system consisting of 188800 elements. The grid size on the horizontal plane (X-Y plane) is 100 m by 100 m. We have

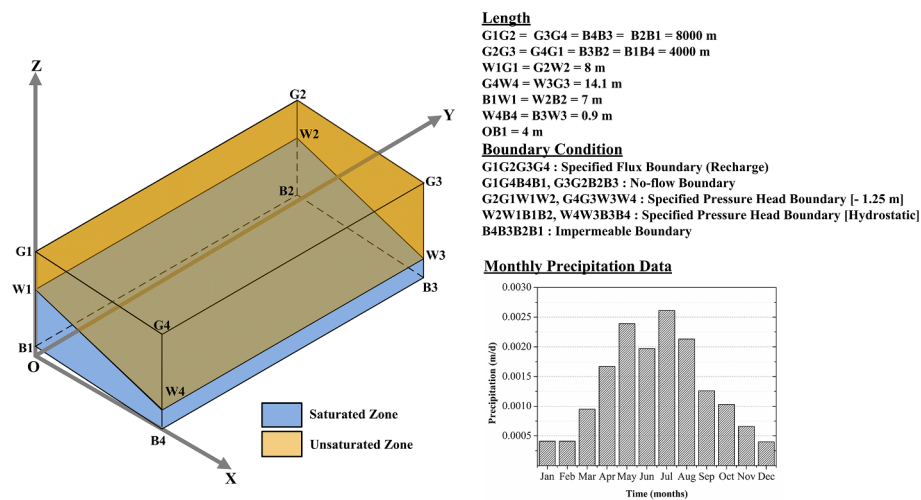


Fig. 5. Schematic diagram of the hypothetical domain and the initial water table considered for TC8.

considered $\Delta z = 0.3\text{ m}$ up to a height of 0.9 m from the bottom in the vertical direction. Above that, we have assumed a constant value of $\Delta z = 0.25\text{ m}$. We have modeled the flow in the unconfined aquifer with

a repetition of the monthly precipitation data (Fig. 5) for 5 years considering $\Delta t_0 = 3600\text{ s}$ and $\Delta t_{max} = 86400\text{ s}$.

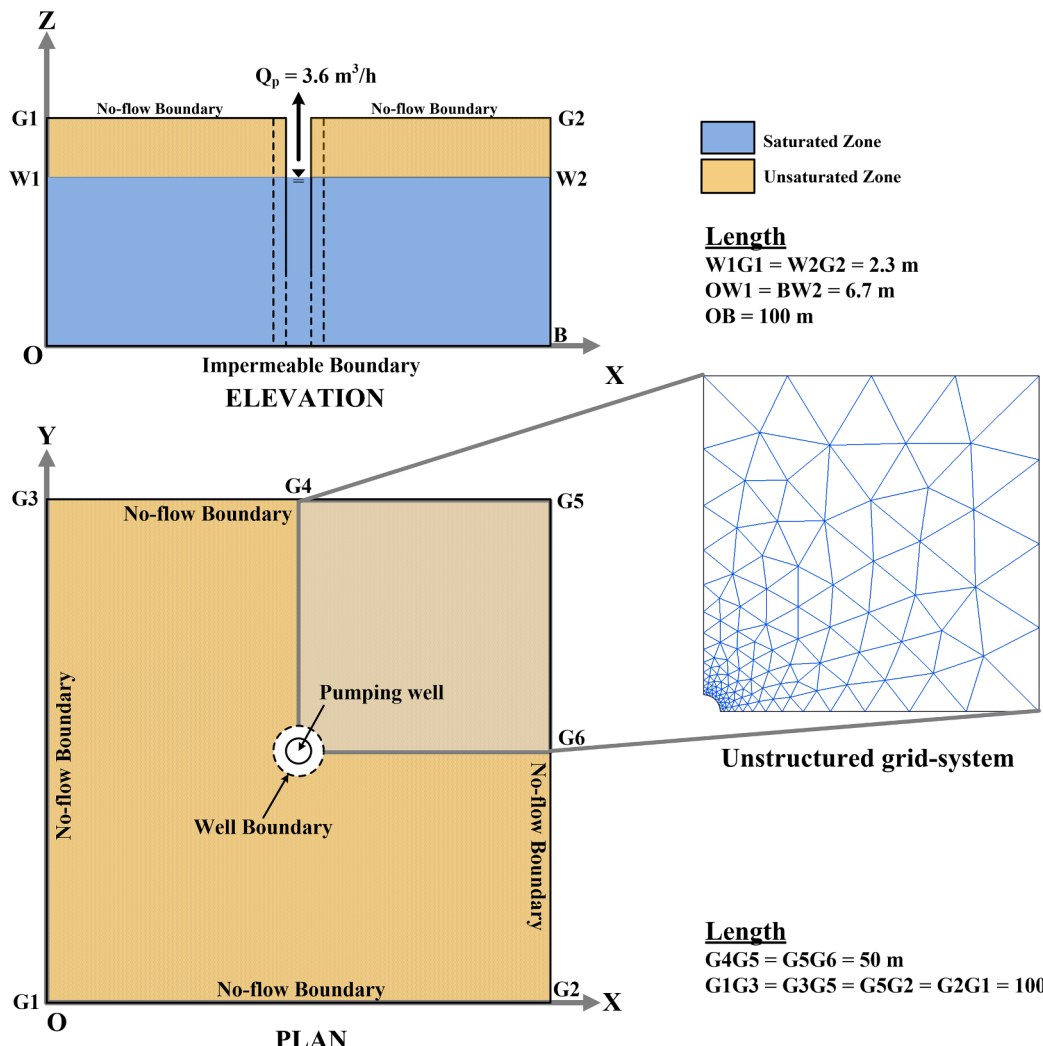


Fig. 6. Schematic diagram showing the plan and elevation of the domain alongside the unstructured grid system for the unconfined aquifer pumping test considered for TC9.

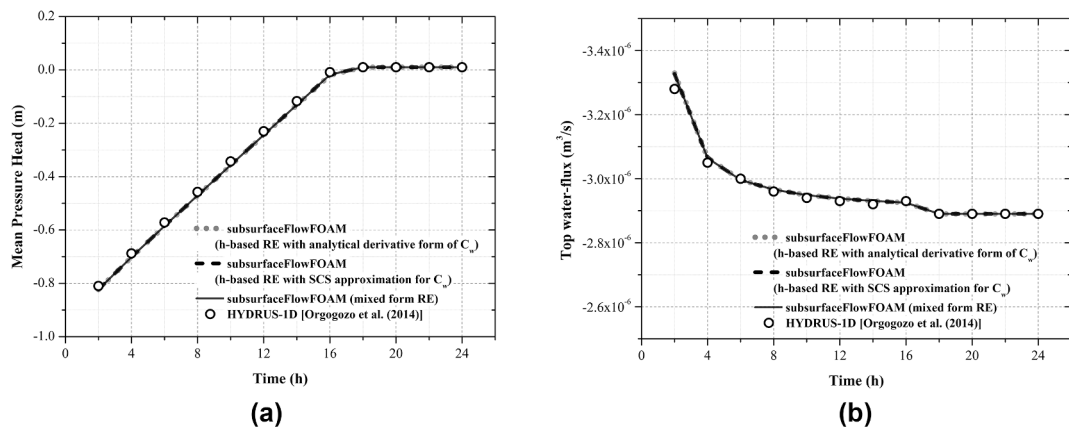


Fig. 7. (a) Comparison between mean pressure head calculated by *subsurfaceFlowFOAM* for TC1 and HYDRUS-1D results of Orgogozo et al. (2014). (b) Comparison between top boundary flux calculated by *subsurfaceFlowFOAM* for TC1 and HYDRUS-1D results of Orgogozo et al. (2014).

5.9. TC9: Three-dimensional field-scale unconfined aquifer pumping test

We have tested the field-scale applicability of *subsurfaceFlowFOAM* by modeling the unconfined aquifer pumping test of Nwankwor et al. (1992). Delayed piezometer response is very significant when the hydraulic head changes rapidly near the pumping well. One of the significant challenges in evaluating the flow dynamics in an unconfined aquifer system due to extraction through a pumping well is addressing the delayed yield effect (Moench, 1997). The estimated drawdown also depends on the diameter of the pumping well. The pumping well is usually considered to be a line source to solve pumping problems in unconfined aquifers. The classical analytical solutions developed by Boulton (1954); Dagan (1967); Neuman (1972); Neuman (1974) considered the pumping well diameter to be infinitesimally small, thereby failing to justify the measured drawdown values at the well and in its vicinity at early times.

In this test case, we have proposed an alternative approach to solving unconfined aquifer pumping problems, considering the diameter of the pumping well to be of finite dimensions. In *subsurfaceFlowFOAM*, we have implemented the Laplace transform solution of dimensionless drawdown for flow to a partially penetrating well of finite diameter in a slightly compressible unconfined aquifer, as presented by Moench (1997). Assuming the homogeneity of aquifer parameters in the vicinity of the pumping well, we have defined a circular time-varying specified pressure head boundary around the well. We have computed the pressure head from the dimensionless drawdown values obtained by numerically inverting the Laplace domain solution (Moench, 1997). We have specified the calculated pressure head on the well-boundary at every time step.

- **Pumping well boundary in an unconfined aquifer:** We have specified the pressure head along the well boundary by the following function:

$$h(\mathbf{x}, t) = z_{wt} - s_{ao} - z \quad (24)$$

The derivation of drawdowns at the well-boundary, s_{ao} and within the pumping well, s_{aw} — are illustrated in Appendix 1. To specify the time-varying pressure head on the well-boundary in an unconfined aquifer, we have developed the boundary condition type *well-UnconfinedBC* in *subsurfaceFlowFOAM*.

The test case considers a square-shaped unconfined aquifer of sides 100 m and depth 9 m with a pumping well of inner diameter 0.15 m located at the center of the aquifer. The pumping well has a well-screen of depth 4 m at the bottom of the aquifer and operates at a constant rate of 3.6 m³/h throughout the 24 h pumping test. The unconfined aquifer is

homogeneous with constant saturated hydraulic conductivity values of 5.7 m/d and 3.6 m/d in horizontal and vertical directions. We have considered specific storage of the aquifer to be $3.25 \times 10^{-4} /m$. The soil-characteristic parameter values considered in this study were calibrated by Akindunni and Gillham (1992), viz. $\theta_s = 0.37$, $\theta_r = 0.07$, $\epsilon = 0.37$, $\alpha_w = 1.9 /m$ and $\beta_w = 6.095$. A thick deposit of clayey silt bounds the aquifer at the bottom, making it an impermeable boundary. We have also considered the other boundaries of the domain as no-flow boundaries. Additionally, the initial water table is at a depth of 2.3 m from the top of the domain. Due to symmetry, we have modeled only a quarter of the study domain (Fig. 6). We have discretized the selected quarter of the domain into an unstructured grid system with 29160 prismatic elements. We have considered the well-boundary at a radial distance of 0.5 m from the center of the pumping well. Initially, we have assumed hydrostatic distribution of pressure head both below and above the water table throughout the domain. With $\Delta t_0 = 1$ s and $\Delta t_{max} = 360$ s, we have performed the simulation for a time span of 24 h.

6. Results and Discussion

We have evaluated the performance of *subsurfaceFlowFOAM* by comparing the numerical results of the considered test cases against the experimental data, analytical solutions, numerical solutions, HYDRUS (1D/2D/3D) simulation results, or measured field data, whenever available. We have also carried out a comparative study between the h-based and mixed-form RE solvers to comment on their accuracy, efficiency, and applicability for solving different variably saturated flow problems.

For TC1, we have compared the time evolution of average pressure head values in the soil column against the HYDRUS 1D results from Orgogozo et al. (2014) in Fig. 7a. We have also compared the temporal changes in water-flux at the top boundary, as shown in Fig. 7b. Figs. 7a & Fig. 7b reveal that the *subsurfaceFlowFOAM* results are in close agreement with the computed values of HYDRUS-1D. Through this example, we have examined the performances of the RE solvers and the effect of discretization of the specific moisture capacity term C_w on their solution accuracy, mass conservation, and computational efficiency. We have compared the pressure head distributions within the soil column after 16 h of simulation, just before the entire soil column attains saturation in Fig. 8a. The solution of the h-based RE solver with SCS approximation for C_w correspond very closely with the mixed-form RE solver solution. However, the results of the h-based RE solver using the analytical derivative of C_w lag behind the results of the other two numerical schemes near the free-drainage bottom boundary. In Fig. 8b, we have shown the comparison of cumulative MBE incurred by the three numerical techniques. As previously stated, the h-based RE solver using the analytical derivative form of C_w is highly inefficient in conserving

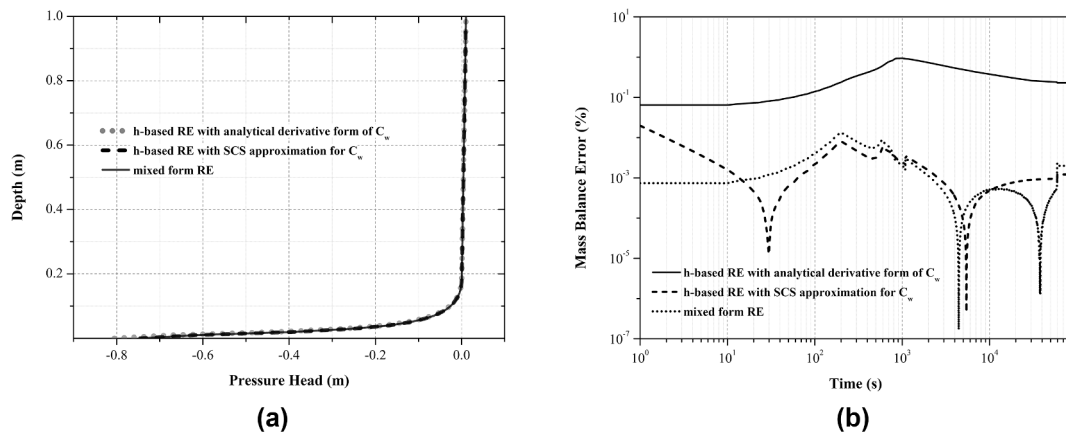


Fig. 8. (a) Comparison among pressure head distributions calculated by the *subsurfaceFlowFOAM* solvers after 16 h for TC1. (b) Comparison among cumulative MBE incurred by the *subsurfaceFlowFOAM* solvers for TC1.

mass relative to the other two numerical schemes. On the contrary, the h-based RE solver with SCS approximation for C_w exhibits high mass balance accuracy. Hence, the cause of mass imbalance can be attributed to the representation of the C_w term, which is the only difference between the two approaches made with the h-based RE solver. It implies that the analytical derivative of C_w fails to preserve the FD approximation of $\frac{\partial \phi}{\partial t}$ employed in the SCS approximation scheme. The mixed-form RE solver shows excellent mass balance accuracy using the analytical derivative of C_w because the term vanishes as the solution approaches convergence for each time-step. Nonetheless, the mass-conservative nature of FV approximation has contributed toward achieving low MBE in all the numerical approaches. For quantifying the computational efficiency, we have evaluated the measure of computational work, which we can illustrate as the following (Rathfelder and Abriola, 1994):

$$W_{comp} = \log_{10}(N_{ts} \times N_{iter}) \quad (25)$$

We have presented the cumulative MBE and the computational work done by the three numerical schemes after 24 h of simulation in Table 3. Looking at Table 3, we can comment that — despite being mass conservative, the mixed-form RE solver is computationally expensive than the h-based solver in terms of both time and work done. Since MBE and the acquired computational expenses depend on initial time-step size, convergence criterion, and time-step adjustment algorithm, we have considered the same values of Δt_0 and Δt_{max} for all the numerical schemes.

For TC2, we have recorded the pressure head values along the length of the column at 1, 2, 4, 10 and 32 h from the commencement of the infiltration process. We have compared the recorded pressure head profiles against the results of Paniconi et al. (1991) in Fig. 9 and have found that they match perfectly with each other. As we have considered hydrostatic pressure head distribution, the soil near the top surface is very dry initially. Hence, the soil near the top boundary where the time-varying flux is specified requires some time to adapt to the imposed boundary condition at initial times. It results in high MBE during the initial time-steps that gradually decrease with time. In our simulation,

we have considered very small Δt_0 , which has facilitated overcoming the inefficiency of the Picard iteration scheme during the initial time-steps as experienced in Paniconi et al. (1991). Despite high mass imbalance at early times, we have achieved cumulative MBE values of $6.13 \times 10^{-1}\%$ and $6.14 \times 10^{-1}\%$ at the end of 32 h of simulation for the h-based (SCS approximation) and mixed-form RE solvers, respectively — demonstrating the mass-conservative nature of *subsurfaceFlowFOAM*.

In TC3, *subsurfaceFlowFOAM* solvers successfully capture the transition from saturated to unsaturated conditions without any issue related to numerical stability and mass conservation. As the simulation commences, water in the initially saturated soil column starts moving down, draining rapidly through the bottom under the action of gravity. As a result, high MBE is observed during the initial few time-steps, which diminishes gradually. Moreover, due to immediate drainage from the bottom of the soil column, instability arises in the system requiring many Picard iterations for convergence. The assumption of $\Delta t_0 = 0.1$ s helps smooth convergence control during this initial period. As this initial phase gets over, the adaptive time-stepping algorithm gradually increases Δt until Δt_{max} is reached. Fig. 10 shows the simultaneous variation of Δt and N_p with time, justifying the effectiveness of the adaptive time-stepping algorithm to ensure smooth convergence at reduced computational expenses. We can attribute the stepped nature of the Δt curves in Fig. 10 to the stabilization technique adopted in the time-stepping algorithm. The stabilization scheme only increases the Δt value if N_p is sufficiently low for 10 successive time-steps, eliminating

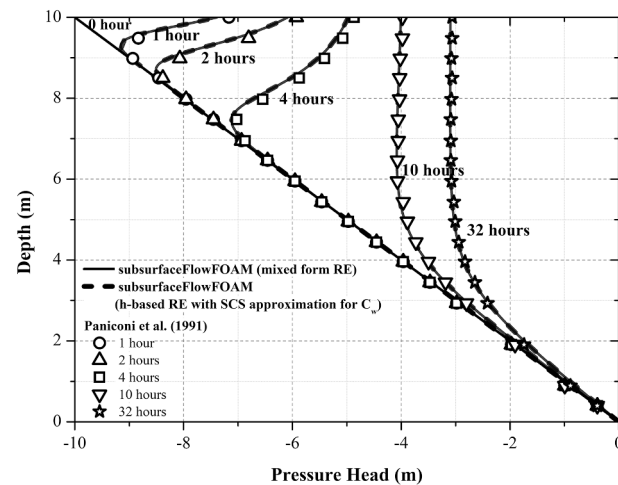


Table 3

Comparison of MBE and computational expenses incurred by different numerical schemes for TC1.

RE Form	C_w approximation Form	Cumulative MBE (%)	CPU Time (s)	W_{comp}
h-based	Analytical derivative	2.29×10^{-1}	7.45	8.08
	SCS approximation	1.21×10^{-3}	6.77	8.07
mixed	—	2.00×10^{-3}	8.44	8.17

Fig. 9. Comparison between pressure head distribution calculated by *subsurfaceFlowFOAM* for TC2 and Paniconi et al. (1991) after 1, 2, 4, 10 & 32 h.

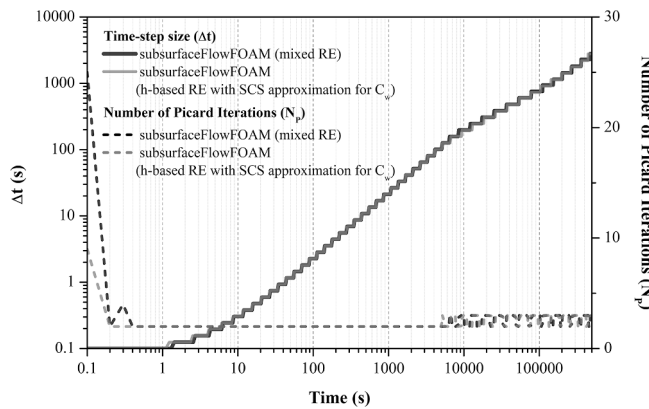


Fig. 10. Variation of Δt and N_p with time for *subsurfaceFlowFOAM* solvers for TC3.

convergence failure. We have compared the *subsurfaceFlowFOAM* results of pressure head and moisture content after 1, 4, 20 and 100 days of simulation with the experimental data of Forsyth et al. (1995) in Fig. 11a & Fig. 11b respectively. The numerical results replicate the experimental values satisfactorily, thereby justifying the potential applicability of *subsurfaceFlowFOAM* for this test case. Additionally, the

cumulative MBE values at the end of 100 days simulation are $2.17 \times 10^{-3}\%$ and $2.13 \times 10^{-3}\%$ respectively for h-based (SCS approximation) and mixed-form RE solvers.

In TC4, we have recorded the pressure head and the moisture content within the heterogeneous soil column after 10 and 20 days of simulation. We have compared these results of *subsurfaceFlowFOAM* with the numerical results presented in Li et al. (2021). Figs. 12a & Fig. 12b claim that the two results are in perfect agreement with each other. As the bottom sand layer is overlain by a clay layer of very low hydraulic conductivity, the change in top boundary flux does not affect any change in moisture content and pressure head of that layer. Due to continuous drainage from the bottom of the soil column, the pressure head within the bottom sand layer decreases steadily for 20 days creating arid soil conditions within that layer. The pressure head and moisture content increase in the top sand layer due to continuous infiltration for the initial 10 days. From 10 to 20 days, the top boundary flux shifts from infiltration to evaporation; thereby, the moisture content and the pressure head decrease within the soil column. Through this study, *subsurfaceFlowFOAM* guarantees its robustness as it nicely adapts to the alternating episodes of infiltration and evaporation imposed on the top boundary without encountering any numerical instability. Both the *subsurfaceFlowFOAM* solvers exhibit smooth solution at the soil layer interfaces without any convergence issues, which is generally experienced by other numerical schemes due to spatial discontinuity among soil-

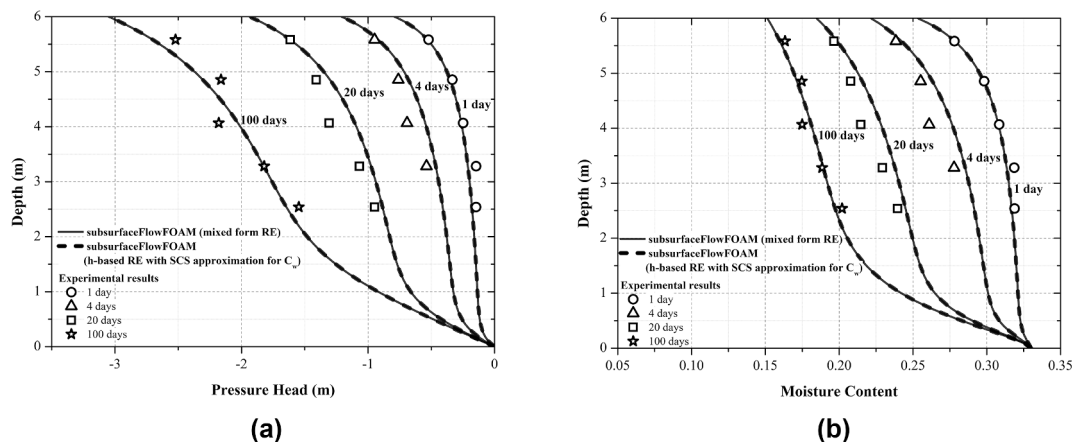


Fig. 11. (a) Comparison between pressure head distribution calculated by *subsurfaceFlowFOAM* for TC3 and experimental results of Forsyth et al. (1995) after 1, 4, 20 & 100 days. (b) Comparison between moisture content distribution calculated by *subsurfaceFlowFOAM* for TC3 and experimental results of Forsyth et al. (1995) after 1, 4, 20 & 100 days.

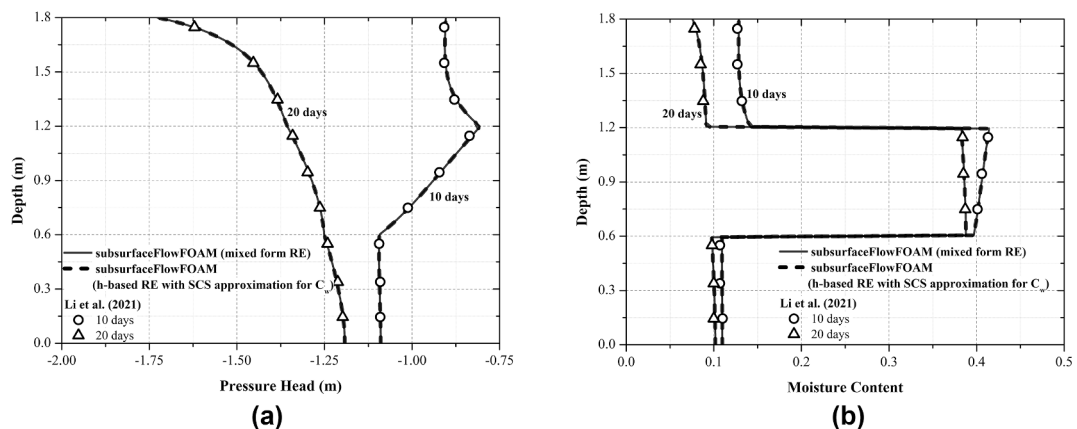


Fig. 12. (a) Comparison between pressure head distribution calculated by *subsurfaceFlowFOAM* for TC4 and Li et al. (2021) after 10 & 20 days. (b) Comparison between moisture content distribution calculated by *subsurfaceFlowFOAM* for TC4 and Li et al. (2021) after 10 & 20 days.

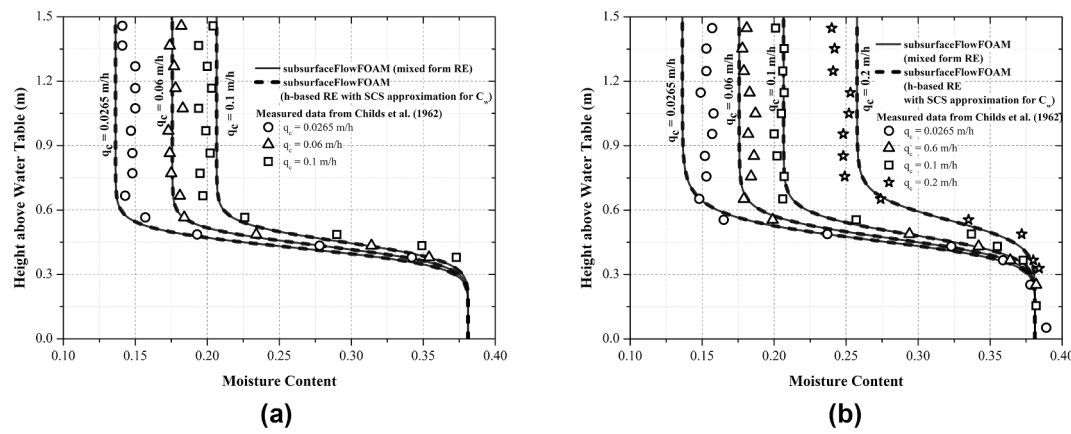


Fig. 13. (a) Comparison between the steady-state moisture content profiles calculated by *subsurfaceFlowFOAM* for TC5 and measured data of [Childs and Poulovassilis \(1962\)](#) when the water table is falling with a velocity of 0.172 m/h for rainfall intensities $0.0265, 0.06$ and 0.1 m/h . (b) Comparison between the steady-state moisture content profiles calculated by *subsurfaceFlowFOAM* for TC5 and measured data of [Childs and Poulovassilis \(1962\)](#) when the water table is falling with a velocity of 0.344 m/h for rainfall intensities $0.0265, 0.06, 0.1$ and 0.2 m/h .

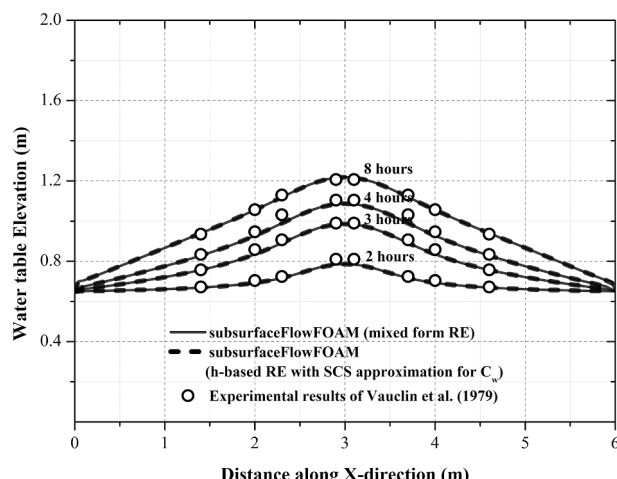


Fig. 14. Comparison between the water table profiles calculated by *subsurfaceFlowFOAM* for TC6 and experimental results of [Vauclin et al. \(1979\)](#) after 2, 3, 4 & 8 h.

characteristic parameters in heterogeneous layered soils. Furthermore, *subsurfaceFlowFOAM* vividly captures the effects of heterogeneity in porous media flow through non-overlapping soil layers yielding highly accurate results with cumulative MBE values as low as $5.38 \times 10^{-4}\%$ and $5.37 \times 10^{-4}\%$ respectively, for h-based (SCS approximation) and mixed-form RE solvers at the end of the simulation period of 20 days.

For TC5, we have recorded the moisture content profile on the attainment of steady-state conditions within the soil column for each simulation. We have accomplished complete steady-state conditions within the soil column approximately after 8 h 44 min and 4 h 22 min from the initiation of the movement of the water table with velocities $v_z = 0.172 \text{ m/h}$ and $v_z = 0.344 \text{ m/h}$, respectively. We have shown the comparison between the simulated and the experimental moisture content profiles for $v_z = 0.172 \text{ m/h}$ and $v_z = 0.344 \text{ m/h}$ at different infiltration rates in Fig. 13a & Fig. 13b respectively. The deviations observed from the measured data are primarily due to the errors incurred in measuring and calibrating the van Genuchten–Mualem soil–water characteristic parameters. Both h-based (SCS approximation) and mixed-form RE solvers have achieved high mass balance accuracy at the end of each simulation with sufficiently low cumulative MBE percentages in the order of 10^{-3} .

As the specific storage S_s is set to zero for TC6, *RichardsFOAM* fails to simulate this problem. Applying *subsurfaceFlowFOAM*, we have

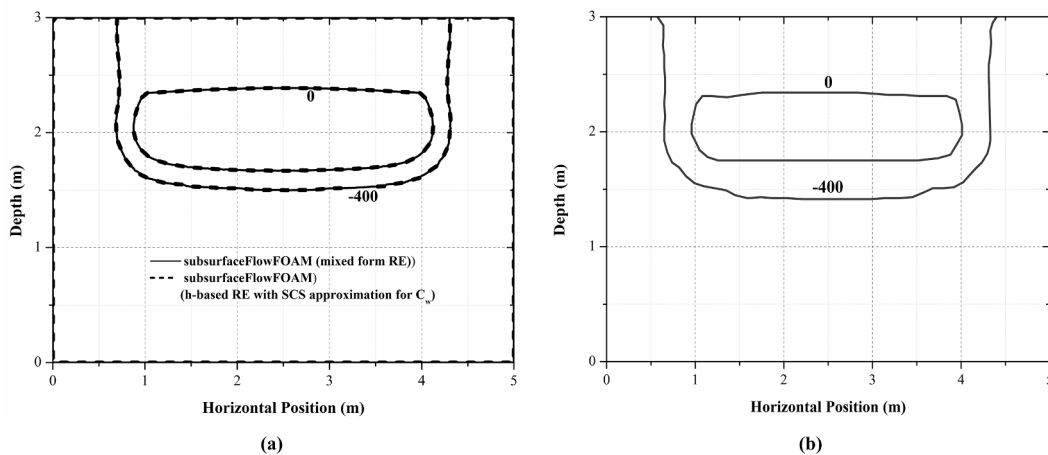


Fig. 15. (a) Comparison between pressure head contours (m) simulated by *subsurfaceFlowFOAM* for TC7 after 24 h. (b) Pressure head contours (m) presented in [Kirkland et al. \(1992\)](#) after 24 h.

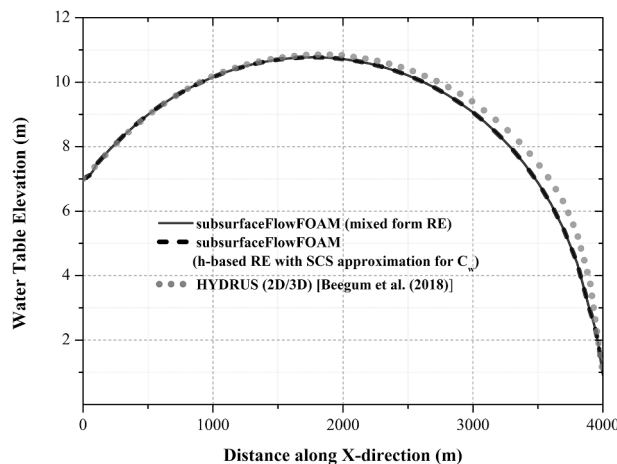


Fig. 16. Comparison between the water table profiles calculated by *subsurfaceFlowFOAM* for TC8 and Beegum et al. (2018) after 5 years.

successfully modeled the spatial and temporal distribution of the phreatic surface in a two-dimensional domain with desirable accuracy and guaranteed mass conservation. A gradual rise in the water table is observed approximately after 1 h 20 min from the onset of simulation when the infiltrated water meets the initial water table flowing down the vadose zone. We have plotted the transient positions of the water table at 2, 3, 4 and 8 h in Fig. 14 and have compared them with the experimental results of Vauclin et al. (1979). Both results are in good agreement with each other. Besides, the cumulative MBE values for the h-based (SCS approximation) and mixed-form RE solvers at the end of 8 h are $3.97 \times 10^{-4}\%$ and $2.79 \times 10^{-5}\%$, respectively.

The simulation of the perched water table problem in TC7 is challenging and requires special attention toward spatial discretization and time-step size selection for convergence. The solution fails to converge if the unstructured grid is generated with an equivalent characteristic length (l_c) greater than 0.1 m. As we have assumed very dry initial conditions with pressure head -500 m, we have started the simulation with $\Delta t_0 = 0.01$ s to avoid convergence failure. We have drawn the pressure head contours of 0 m and -400 m after 24 h of continuous infiltration in Fig. 15a. The contours agree quite well with the results of Kirkland et al. (1992) presented in Fig. 15b. The top sand layer is bounded by a clay layer of very low permeability on its left, right, and

Table 4

Comparison of grid-convergence of *subsurfaceFlowFOAM* for TC1, TC7 & TC9.

Test Case	Description	N _{ele}	Maximum Relative Difference	Cumulative MBE (%)
TC1	Mean Pressure head	100	–	1.90×10^{-3}
		1000	3.74×10^{-1}	2.52×10^{-3}
		10000	6.56×10^{-3}	2.69×10^{-3}
TC7	Pressure head at (2.5, 0, 2.5)	21970	–	1.57×10^{-2}
		87328	3.79×10^{-1}	3.86×10^{-2}
TC9	Drawdown at a radial distance of 5 m	348436	2.20×10^{-1}	5.70×10^{-2}
		29160	–	8.18×10^{-3}
		77940	1.38×10^{-2}	7.87×10^{-3}
		225360	7.97×10^{-3}	7.47×10^{-3}

bottom, the vertical movement of infiltrated water is obstructed, and water starts to get deposited above the clay layer. A smooth pressure gradient is observed within the clay layer with the top and bottom interfaces at pressures of 0 m and -500 m, respectively. A water table starts developing locally much above the impervious bottom boundary approximately after 16 h from the commencement of infiltration. If the infiltration process is ceased, the water table will gradually disappear with time as water will slowly percolate vertically downward into the bottom sand layer through the clay zone. Such temporary formations of the local water table are quite common in natural hydrogeologic systems, and the capability of the *subsurfaceFlowFOAM* solvers in simulating perched water table problem advocate their robustness. Moreover, we have achieved very low cumulative MBE values of $4.64 \times 10^{-3}\%$ and $1.57 \times 10^{-2}\%$ with the h-based (SCS approximation) and the mixed-form RE solvers respectively.

The example considered in TC8 is an extension of the water table recharge problem in the three-dimensional domain. To reduce the simulation time, we have performed parallel computation using four processors. We have displayed the water table profile at the end of 5 years in Fig. 16. The estimated water table profile matches closely with the profile predicted by Beegum et al. (2018) using HYDRUS (2D/3D) till midway along the length of the domain. However, *subsurfaceFlowFOAM* underestimates the recessing curvature of the phreatic surface compared to HYDRUS (2D/3D) results presented by Beegum et al. (2018). The difference between the two profiles increases as we approach the right boundary with a maximum variation of 0.91 m

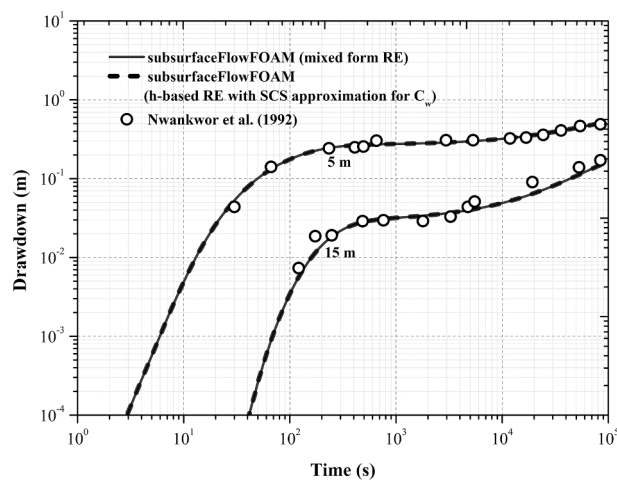


Fig. 17. Comparison between the drawdown values calculated by *subsurfaceFlowFOAM* for TC9 and field data of Nwankwor et al. (1992) after 24 h of pumping.

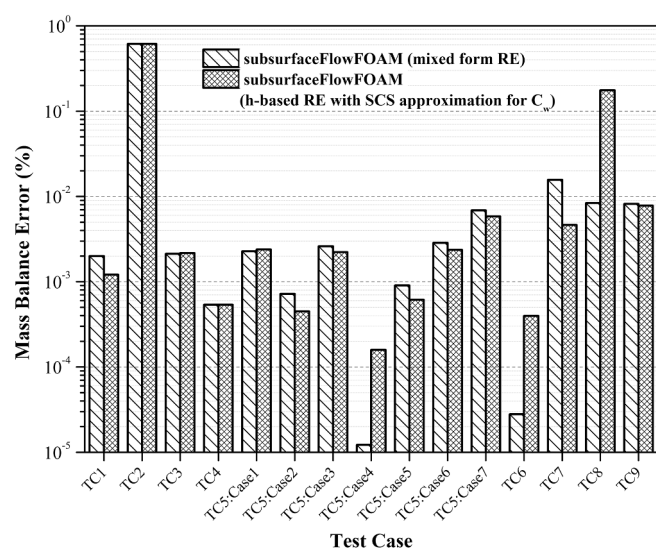


Fig. 18. Comparison of the cumulative MBE values at the end of simulation for all the test cases.

Table 5

Comparison of computation time for all the considered test cases.

Test Case	Grid type	N _{ele}	T _f (d)	Δt ₀ (s)	Δt _{max} (s)	CPU Time (s) (mixed-form RE)	CPU Time (s) (h-based RE with SCS approximation for C _w)
TC1	Structured	100	1	1	3600	8.44	6.77
TC2	Structured	1000	1.33	1	20	17.36	13.77
TC3	Structured	600	100	0.1	3600	8.28	7.39
TC4	Structured	360	20	1	20	149.88	127.86
TC5:Case1	Structured	300	0.36	1	20	2.08	1.78
TC5:Case2	Structured	300	0.36	1	20	2.63	1.98
TC5:Case3	Structured	300	0.36	1	20	2.39	2.06
TC5:Case4	Structured	300	0.18	1	20	1.34	1.08
TC5:Case5	Structured	300	0.18	1	20	1.33	1.13
TC5:Case6	Structured	300	0.18	1	20	1.27	1.11
TC5:Case7	Structured	300	0.18	1	20	1.19	1.05
TC6	Structured	2400	0.33	1	360	33.02	28.48
TC7	Unstructured	21970	1	0.01	20	783.19	712.19
TC8	Structured	188800	1825	3600	86400	928.09	880.36
TC9	Unstructured	29160	1	1	360	66.70	58.36

occurring 100 m inward of the right boundary. We have achieved reasonably low cumulative MBE values of $1.76 \times 10^{-1}\%$ and $8.37 \times 10^{-3}\%$ respectively for the h-based (SCS approximation) and mixed-form RE solvers at the end of 5 years simulation period.

The simulation of the unconfined aquifer test studied in TC9 is beyond the capability of *RichardsFOAM* since the flow domain is anisotropic. We have recorded the temporal variation of pressure head at a depth of 7 m from the top and at radial distances of 5 m and 15 m from the center of the pumping well applying *subsurfaceFlowFOAM*. We have compared the estimated drawdowns with the field data extracted from the time-drawdown curves of [Nwankwor et al. \(1992\)](#) in [Fig. 17](#). The results of *subsurfaceFlowFOAM* correspond well with the measured values addressing the delayed yield effect that arise in the vicinity of the pumping well in an unconfined aquifer. Conventionally, a pumping well is treated as a singular point source in groundwater modeling. Pumping wells encountered in practice are minimal radii in the range of 0.1–0.2 m. Since the well and the domain scales differ significantly, representing a well with the actual radius on a grid system results in issues related to grid orthogonality, aspect ratio, and skewness. On the other hand, grid-convergence issues arise in drawdown calculation if we assume the effective well radius calculated by a well-model ([Dey and Dhar, 2020](#)). Therefore, the actual well radius specification is essential for numerical modeling of pumping tests in unconfined aquifers. The proposed methodology calculates the pressure head on the well-boundary considering the actual radius of the pumping well, thereby fulfilling the grid-convergence criterion for drawdown within the well. Additionally, the methodology successfully conserves mass with cumulative MBE values of $1.64 \times 10^{-2}\%$ and $2.42 \times 10^{-2}\%$ respectively, for the h-based (SCS approximation) and mixed-form RE solvers at the end of 24 h simulation.

We have examined the grid-convergence characteristics of *subsurfaceFlowFOAM* using the examples presented in TC1 (one-dimensional), TC7 (two-dimensional), and TC9 (three-dimensional). We have parametrized the increase in solution accuracy with spatial grid-refinement by calculating the difference between the simulated results for two levels of grid-refinement relative to the simulated results for the coarser grid. We have investigated the grid-convergence characteristics for three levels of grid-refinement for each of the above test cases. A summary of the grid-convergence study for TC1, TC7, and TC9 is presented in [Table 4](#). For TC1, we have run the simulation for vertical step sizes of 10^{-2} , 10^{-3} , and 10^{-4} m to inspect the increase in solution accuracy. We have compared the evolution of the mean pressure head with time in the soil column for the three levels of vertical discretization. For the examples considered in TC7 and TC9, we have performed three

levels of spatial discretization of the respective domains into unstructured grid systems. The unstructured grids were generated using characteristic lengths (l_c) of 0.04, 0.02, and 0.01 m for TC7 and 12.5, 6.25 and 3.125 m for TC9. We have compared the temporal variations in pressure head at (2.5, 0, 2.5) for the three levels of spatial discretization for the perched water table problem. On the other hand, we have analyzed the drawdowns at a radial distance of 5 m from the center of the pumping well at different times for the three levels of the unstructured grid system in the unconfined aquifer pumping test. The results in [Table 4](#) reveal a distinct increase in solution accuracy with finer spatial discretization, thereby satisfying the grid-convergence criteria for any numerical scheme. Moreover, we have also observed that with grid-refinement, there is a marked decrease in the number of iterations (N_p) required for convergence of the Picard iteration scheme. In TC7, for the first discretization level ($l_c = 0.04$) approximately 8.47% of the total time-steps required more than 3 Picard iterations for convergence. However, for the other two discretization levels ($l_c = 0.02, 0.01$) convergence was achieved within 3 Picard iterations for all time-steps. In TC9, *subsurfaceFlowFOAM* solvers converged within 3 Picard iterations for all the three spatial discretization levels. The percentage of the time-steps that converged within 2 Picard iterations increased from 45.17% to 52.36% after the first level of grid-refinement and finally to 62.62% after the second level of grid-refinement. Nonetheless, we have not observed any considerable variation in the order of mass balance accuracy with changing grid dimensions for the examined test cases.

7. Conclusions

In this research work, we have presented a generalized FV-based numerical model, *subsurfaceFlowFOAM* to model subsurface flow through heterogeneous porous media. We have developed mass-conservative solvers for both h-based and mixed forms of RE. Both the solvers estimate the subsurface flow dynamics with desirable accuracy for the considered test cases. Another important aspect of this study is the ability of the solvers to conserve global mass during simulation. In all the test cases, the cumulative MBE is less than the desirable limit of 1% for both the *subsurfaceFlowFOAM* solvers under the conservative property of the FV method. We have presented the comparative representation of the acquired cumulative MBE in [Fig. 18](#). The comparison between the MBE percentages incurred by two *subsurfaceFlowFOAM* solvers reveals that both are efficient at conserving the global mass of water within the flow system. The SCS approximation of the C_w term adopted for the h-based RE solver successfully overcomes the non-conservative nature of the h-based RE producing results with high

mass balance accuracy. The computation time for all the test cases tabulated in Table 5 reveals that the h-based solver is marginally faster between the two solvers. The test problems simulated in this study do not involve large-scale simulations to utilize the benefits of a parallel solver. However, the parallelization strategies embedded in OpenFOAM® are sufficient to establish the advantages of applying *subsurfaceFlowFOAM* to solve regional-scale problems on large time scales ranging in the orders of decades and centuries.

The behavior of the solution of RE constantly varies throughout the simulation period due to the strong nonlinearity of the involved parameters. An assumption of uniform Δt is inappropriate for an RE solver. Implementation of the stabilized and adaptive time-stepping algorithm adjusts the time-step size (Δt) dynamically following the changing hydrological conditions. Initially, the pressure head changes drastically within the system due to imposed initial and boundary conditions. Hence, we have initiated the simulation with a small value of Δt for all the test cases to ensure smooth convergence. As the system stabilized or approached steady-state conditions, the algorithm has increased the value of Δt to preserve the computational efficiency of the solver. While simulating the considered test cases, we have not encountered any convergence or numerical instability issue.

The primary objective of this study is to develop a generalized RE solver to model a wide variety of subsurface flow problems ranging from laboratory-scale experiments to watershed-scale regional studies, equipped with advanced computation facilities of parallelization. The advantage of developing the solvers in a universally acclaimed open-source framework like OpenFOAM® is that the computer program becomes easily accessible to other users. On the other hand, standard library operators and functions make the computer program readily interpretable among practitioners, enhancing its applicability to practical problems. In conclusion, the performance evaluation of *subsurfaceFlowFOAM* proves its potential applicability at simulating subsurface flow through homogeneous and heterogeneous porous media on both laboratory and regional scales.

Source Code Availability

The source code can be downloaded from the link: <https://github.com/gwres/subsurfaceFlowFOAM>

Notations

- C_w = Specific moisture capacity. $[L^{-1}]$
- d = Depth of the top of the well-screen below the initial water table. $[L]$
- d_s = Thickness of the well-bore skin. $[L]$
- F_ϕ = Flux normal to the face of an element. $[L^3 T^{-1}]$
- h = Pressure head. $[L]$
- h_c = Known pressure head function. $[L]$
- \mathbf{K} = Hydraulic conductivity tensor. $[LT^{-1}]$
- K_r = Hydraulic conductivity in the horizontal direction. $[LT^{-1}]$
- \mathbf{K}_s = Saturated hydraulic conductivity tensor. $[LT^{-1}]$
- K_{sw} = Hydraulic conductivity of the well-bore skin. $[LT^{-1}]$
- K_z = Hydraulic conductivity in the vertical direction. $[LT^{-1}]$
- K_0 = Zero-order modified Bessel function of second kind.
- K_1 = First-order modified Bessel function of second kind.
- l = Depth of the bottom of the well-screen below the initial water table. $[L]$
- N_{bf} = Number of boundary faces in the domain of interest.
- N_{ele} = Number of elements in the domain of interest.
- N_{iter} = Total number of iterations.
- N_p = Number of Picard iterations required for convergence at any time-step.
- N_{pl}, N_{pu} = Lower and upper limits of the number of Picard iterations respectively for effecting a change in time-step size.
- N_{pmax} = Maximum number of allowable Picard iterations.
- N_S = Number of terms used in the Stehfest algorithm.
- $N_{St_{max}}$ = Maximum number of stabilization counters for adaptive time-stepping algorithm.
- N_{ts} = Number of time-steps.
- $\hat{\mathbf{n}}$ = Normal vector at the boundary.
- Q_p = Volumetric extraction rate of the pumping well. $[L^3 T^{-1}]$
- q_c = Known flux function. $[LT^{-1}]$
- q_s = Internal source or sink term. $[L^3 T^{-1} L^{-3}]$
- r = Radial distance of the well boundary from centre of the pumping well. $[L]$
- r_w = Radius of the pumping well. $[L]$
- r_{wc} = Inside radius of the pumped well in the interval where water levels change during pumping. $[L]$
- S_e = Degree of saturation. $[M^0 L^0 T^0]$
- S_s = Specific storage. $[L^{-1}]$
- S_y = Specific yield. $[M^0 L^0 T^0]$
- s_{ao} = Drawdown at the well boundary. $[L]$
- s_{aw} = Drawdown at the pumping well. $[L]$
- \bar{s}_{aoD} = Laplace transform of dimensionless drawdown at the well boundary. $[M^0 L^0 T^0]$
- \bar{s}_{awD} = Laplace transform of dimensionless drawdown at the pumping well. $[M^0 L^0 T^0]$
- s_c = Stabilization counter for adaptive time-stepping algorithm.
- T_f = Final solution time. $[T]$
- t = Time coordinate. $[T]$
- V = Volume of an element. $[L^3]$
- v_z = Velocity of the moving water table. $[LT^{-1}]$
- W = Weighting coefficients in Stehfest algorithm.
- W_{comp} = Measure of computational work.
- \mathbf{x} = Vector of space coordinates in the Euclidean space. $[L]$
- z = Vertical coordinate. (positive upward from the bottom of the domain) $[L]$
- z_{ao} = Hydraulic head at the well boundary. $[L]$
- z_{aw} = Hydraulic head at the pumping well. $[L]$
- z_{wt} = Height of the water table above the bottom of the domain. $[L]$
- γ_{water} = Unit weight of water on Earth at 4°C. $[ML^{-2} T^{-2}]$
- Δt = Time-step size. $[T]$
- $\Delta t_{min}, \Delta t_{max}$ = Minimum and maximum time-step size respectively. $[T]$
- Δt_0 = Initial time-step size. $[T]$
- $\Delta x, \Delta z$ = Grid size in X and Z directions respectively. $[L]$
- δ_f = Time-step adjustment factor.
- $\delta_{h_{rel}}$ = Relative tolerance for Mixed pressure head convergence criterion. $[L]$
- $\delta_{h_{tol}}$ = Tolerance for Standard pressure head convergence criterion. $[L]$
- $\delta_{\theta_{tol}}$ = Tolerance for Standard moisture content convergence criterion. $[M^0 L^0 T^0]$
- η = Porosity of the medium. $[M^0 L^0 T^0]$
- θ = Moisture content. $[M^0 L^0 T^0]$
- θ_r = Residual moisture content. $[M^0 L^0 T^0]$
- θ_s = Saturated moisture content. $[M^0 L^0 T^0]$
- α = Compressibility of the porous medium. $[M^{-1} LT^2]$
- α_{uc} = Empirical drainage constant. $[T^{-1}]$
- α_w = Soil-specific coefficient equivalent to the capillary length scale. $[L^{-1}]$
- β = Compressibility of water. $[M^{-1} LT^2]$
- β_w = Soil-specific exponent. $[M^0 L^0 T^0]$
- Ω = Physical domain.

CRediT authorship contribution statement

Saumava Dey: Conceptualization, Methodology, Validation, Writing - original draft. **Anirban Dhar:** Supervision, Writing - review & editing.

Declaration of Competing Interest

The authors declare that they have no known competing financial

interests or personal relationships that could have appeared to influence the work reported in this paper.

Appendix A

This appendix provides the steps involved in the computation of drawdown s_{ao} at the well boundary given in Eq. (24). The expressions for the dimensionless parameters used in drawdown calculation are presented in Table 6. We can calculate the Laplace transform of the dimensionless drawdown \bar{s}_{aoD} at a radial distance r from the center of the pumping well as:

$$\bar{s}_{aoD}(r_D, z_D, p_{uc}) = \frac{2E_{uc}}{p_{uc}(l_D - d_D)[1 + W_D p_{uc}(A_{uc} + S_w)]} \quad (\text{A.1})$$

where,

$$A_{uc} = \frac{\frac{2}{(l_D - d_D)} \sum_{n=0}^{\infty} K_0(q_{1n}) \{ \sin[\epsilon_n(1 - d_D)] - \sin[\epsilon_n(1 - l_D)] \}^2}{\epsilon_n q_{1n} K_1(q_{1n}) [\epsilon_n + 0.5 \sin(2\epsilon_n)]} \quad (\text{A.2})$$

$$E_{uc} = \frac{2 \sum_{n=0}^{\infty} K_0(q_{2n}) \cos(\epsilon_n z_D) \{ \sin[\epsilon_n(1 - d_D)] - \sin[\epsilon_n(1 - l_D)] \}}{q_{1n} K_1(q_{1n}) [\epsilon_n + 0.5 \sin(2\epsilon_n)]} \quad (\text{A.3})$$

$$q_{1n} = (p_{uc} + \epsilon_n^2 \beta_{ucD})^{0.5} \quad (\text{A.4})$$

$$q_{2n} = q_{1n} r_D \quad (\text{A.5})$$

and ϵ_n are the roots of:

$$\epsilon_n \tan(\epsilon_n) = \frac{p_{uc}}{\sigma_{uc} \beta_{ucD} + \frac{p_{uc}}{\gamma_{uc}}}, \quad n = 1, 2, 3, \dots, \infty \quad (\text{A.6})$$

We have computed the summations in Eqs. (A.2) and (A.3) for N_C terms where, N_C can be evaluated as:

$$N_C = \max\{N_{C\min}, \min\{N_{C\max}, N_{C\max} 2^{\lceil -\log_{10}(\beta_{uc}) - 2 \rceil}\}\} \quad (\text{A.7})$$

In this paper, we have assumed the values of $N_{C\min}$ and $N_{C\max}$ as 4 and 30 respectively.

To evaluate the dimensionless drawdown s_{aoD} at the well boundary, we have performed numerical inversion of the Laplace domain solution given in Eq. (A.1) applying Stehfest algorithm (Stehfest, 1970). Stehfest algorithm calculates the dimensionless drawdown s_{aoD} as follows:

Table 6

Dimensionless parameters and expressions involved in drawdown calculation for unconfined aquifer pumping test.

Dimensionless Parameter	Expression
r_{WD}	$\frac{r_w}{z_{wt}}$
r_D	$\frac{r_w}{l}$
z_D	$\frac{r_w}{z}$
l_D	$\frac{z_{wt}}{l}$
d_D	$\frac{z_{wt}}{d}$
t_D	$\frac{z_{wt}}{K_r t}$
β_{ucD}	$\frac{r_w^2 S_s}{K_z r_w D^2}$
β_{uc}	$\frac{K_r}{\beta_{ucD} r_D^2}$
γ_{uc}	$\frac{\alpha_{uc} z_{wt} S_y}{a_{uc} z_{wt}}$
σ_{uc}	$\frac{K_s}{S_y z_{wt}}$
S_w	$\frac{S_y}{K_r d_s}$
W_D	$\frac{K_{sw} r_w}{r_{wc}^2}$
s_{aoD}	$\frac{2r_w^2 S_s (l - d)}{4\pi K_r z_{wt} (z_{wt} - z_{ao})}$
s_{awD}	$\frac{Q_p}{4\pi K_r z_{wt} (z_{wt} - z_{aw})}$

$$s_{aoD}(t_D) = \frac{\ln 2}{t_D} \sum_{j=1}^{N_S} W_j \bar{s}_{aoD}(r_D, z_D, p_{uc}) \quad (\text{A.8})$$

where,

$$p_{uc} = j \frac{\ln 2}{t_D} \quad (\text{A.9})$$

$$W_j = (-1)^{\binom{N_S}{2} + j} \sum_{k=\frac{j+1}{2}}^{\min\left(j, \frac{N_S}{2}\right)} \frac{k^{\binom{N_S}{2}} 2k!}{\left(\frac{N_S}{2} - k\right)! k! (k-1)! (j-k)! (2k-j)!} \quad (\text{A.10})$$

Moreover, we can calculate the Laplace domain solution of the dimensionless drawdown in the pumping well as follows:

$$\bar{s}_{awD}(p_{uc}) = \frac{2(A_{uc} + S_w)}{p_{uc}(l_D - d_D)[1 + W_D p_{uc}(A_{uc} + S_w)]} \quad (\text{A.11})$$

We can evaluate the dimensionless drawdown at the pumping well s_{awD} using the Stehfest algorithm similarly as done for the well-boundary in Eqs. (A.8)–(A.10).

References

- Abbeel, W.V., 3 1984. Hydraulic testing of crushed Bandelier Tuff. Tech. rep., LA-10037-MS. Los Alamos National Laboratory, Los Alamos, NM.
- Akindunni, F.F., Gillham, R.W., 1992. Unsaturated and saturated flow in response to pumping of an unconfined aquifer: Numerical investigation of delayed drainage. *Groundwater* 30 (6), 873–884.
- Allen, M.B., Murphy, C., 1985. A finite element collocation method for variably saturated flows in porous media. *Numerical Methods for Partial Differential Eqs.* 1 (3), 229–239.
- Allen, M.B., Murphy, C.L., 1986. A finite-element collocation method for variably saturated flow in two space dimensions. *Water Resour. Res.* 22 (11), 1537–1542.
- Aravena, J.E., Dussaillant, A., 2009. Storm-water infiltration and focused recharge modeling with finite-volume two-dimensional richards equation: Application to an experimental rain garden. *Journal of Hydraulic Engineering* 135 (12), 1073–1080.
- Ashby, S.F., Falgout, R.D., 1996. A parallel multigrid preconditioned conjugate gradient algorithm for groundwater flow simulations. *Nucl. Sci. Eng.* 124 (1), 145–159.
- Beegum, S., Simunek, J., Szymkiewicz, A., Sudheer, K.P., Nambi, I.M., 2018. Updating the Coupling Algorithm between HYDRUS and MODFLOW in the HYDRUS Package for MODFLOW. *Vadose Zone Journal* 17 (1), 1–8.
- Berardi, M., Difonzo, F., Lopez, L., 2020. A mixed mol-tmol for the numerical solution of the 2d richards' equation in layered soils. *Computers & Mathematics with Applications* 79 (7), 1990–2001.
- Berninger, H., Kornhuber, R., Sander, O., 2015. A multidomain discretization of the richards equation in layered soil. *Computational Geosciences* 19 (1), 213–232.
- Boulton, N.S., 1954. Unsteady radial flow to a pumped well allowing for delayed yield from storage. *Int. Assoc. Sci. Hydrol. Publ.* 2, 472–477.
- Brandt, A., Bresler, E., Diner, N., Ben-Asher, I., Heller, J., Goldberg, D., 1971. Infiltration from a trickle source: I. mathematical models. *Soil Sci. Soc. Am. J.* 35 (5), 675–682.
- Brooks, R.H., Corey, A.T., 1964. Hydraulic Properties of Porous Media. Tech. rep., Colorado State Univ, Fort Collins, Colorado.
- Brooks, R.H., Corey, A.T., 1966. Properties of Porous Media Affecting Fluid Flow. J. Irrigation Drainage Division 92 (2), 61–88.
- Brunner, P., Simons, C.T., 2012. Hydrogeosphere: a fully integrated, physically based hydrological model. *Groundwater* 50 (2), 170–176.
- Brutsaert, W.F., 1971. A functional iteration technique for solving the richards equation applied to two-dimensional infiltration problems. *Water Resour. Res.* 7 (6), 1583–1596.
- Camporese, M., Paniconi, C., Putti, M., Orlandini, S., 2010. Surface-subsurface flow modeling with path-based runoff routing, boundary condition-based coupling, and assimilation of multisource observation data. *Water Resour. Res.* 46 (2).
- Celia, M.A., Bouloutas, E.T., Zarba, R.L., 1990. A General Mass-Conservative Numerical Solution for the Unsaturated Flow Equation. *Water Resour. Res.* 26 (7), 1483–1496.
- Childs, E.C., Poulouvassilis, A., 1962. The Moisture Profile Above a Moving Water Table. *J. Soil Sci.* 13 (2), 271–285.
- Clement, T.P., Wise, W.R., Molz, F.J., 1994. A physically based, two-dimensional, finite-difference algorithm for modeling variably saturated flow. *J. Hydrol.* 161, 71–90.
- Cooley, R.L., 1971. A finite difference method for unsteady flow in variably saturated porous media: Application to a single pumping well. *Water Resour. Res.* 7 (6), 1607–1625.
- Cooley, R.L., 1983. Some new procedures for numerical solution of variably saturated flow problems. *Water Resour. Res.* 19 (5), 1271–1285.
- Coumou, D., Matthäi, S., Geiger, S., Driesner, T., 2008. A parallel fe-fv scheme to solve fluid flow in complex geologic media. *Computers Geosci.* 34 (12), 1697–1707.
- Dagan, G., 1967. A method of determining the permeability and effective porosity of unconfined anisotropic aquifers. *Water Resour. Res.* 3 (4), 1059–1071.
- Dane, J.H., Mathis, F.H., 1981. An adaptive finite difference scheme for the one-dimensional water flow equation. *Soil Sci. Soc. Am. J.* 45 (6), 1048–1054.
- Day, P.R., Luthin, J.N., 1956. A numerical solution of the differential equation of flow for a vertical drainage problem. *Soil Sci. Soc. Am. J.* 20 (4), 443–447.
- Deng, B., Wang, J., 2017. Saturated-unsaturated groundwater modeling using 3d richards equation with a coordinate transform of nonorthogonal grids. *Appl. Math. Model.* 50, 39–52.
- Dey, S., Dhar, A., 2020. On proper orthogonal decomposition (POD) based reduced-order modeling of groundwater flow through heterogeneous porous media with point source singularity. *Adv. Water Resour.* 144 (10), 103703.
- Dogan, A., 1999. Variably saturated three-dimensional rainfall-driven groundwater pumping model. Ph.D. thesis, Dept. of Civil and Coastal Engineering, University of Florida, Gainesville, Florida.
- Dogan, A., Motz, L.H., 2005. Saturated-Unsaturated 3d Groundwater Model. i: Development. *J. Hydrol. Eng.* 10 (6), 492–504.
- Dogan, A., Motz, L.H., 2005. Saturated-Unsaturated 3d Groundwater Model. i: Verification and Application. *J. Hydrol. Eng.* 10 (6), 505–515.
- Eymard, R., Gutnic, M., Hilhorst, D., 1999. The finite volume method for richards equation. *Comput. Geosci.* 3 (3), 259–294.
- Farthing, M.W., Ogden, F.L., 2017. Numerical Solution of Richards' Equation: A Review of Advances and Challenges. *Soil Sci. Soc. Am. J.* 81 (6), 1257–1269.
- Finsterle, S., Doughty, C., Kowalsky, M.B., Moridis, G.J., Pan, L., Xu, T., Zhang, Y., Pruess, K., 2008. Advanced vadose zone simulations using tough. *Vadose Zone J.* 7 (2), 601–609.
- Forsyth, P.A., Wu, Y.S., Pruess, K., 1995. Robust numerical methods for saturated-unsaturated flow with dry initial conditions in heterogeneous media. *Adv. Water Resour.* 18 (1), 25–38.
- Freeze, R.A., 1969. The mechanism of natural ground-water recharge and discharge: 1. one-dimensional, vertical, unsteady, unsaturated flow above a recharging or discharging ground-water flow system. *Water Resour. Res.* 5 (1), 153–171.
- Freeze, R.A., 1971. Three-dimensional, transient, saturated-unsaturated flow in a groundwater basin. *Water Resour. Res.* 7 (2), 347–366.
- Gao, Y., Pu, S., Zheng, C., Yi, S., 2019. An improved method for the calculation of unsaturated-saturated water flow by coupling the fem and fdm. *Sci. Rep.* 9 (1), 1–9.
- Haverkamp, R., Vauclin, M., 1981. A comparative study of three forms of the richard equation used for predicting one-dimensional infiltration in unsaturated soil. *Soil Sci. Soc. Am. J.* 45 (1), 13–20.
- Haverkamp, R., Vauclin, M., Touma, J., Wierenga, P.J., Vachaud, G., 1977. A comparison of numerical simulation models for one-dimensional infiltration. *Soil Sci. Soc. Am. J.* 41 (2), 285–294.
- Healy, R.W., 1990. Simulation of Solute Transport Invariably Saturated Porous Media with Supplemental Information on Modifications to the US Geological Survey's Computer Program VS2D, Vol. 90. Department of the Interior, US Geological Survey.
- Healy, R.W., 2008. Simulating water, solute, and heat transport in the subsurface with the vs2d software package. *Vadose Zone J.* 7 (2), 632–639.
- Herbst, M., Gottschalk, S., Reiβel, M., Hardelauf, H., Kasteel, R., Javaux, M., Vanderborght, J., Vereecken, H., 2008. On preconditioning for a parallel solution of the richards equation. *Computers Geosci.* 34 (12), 1958–1963.
- Horgue, P., Soulaine, C., Franc, J., Guibert, R., Debenest, G., 2015. An open-source toolbox for multiphase flow in porous media. *Comput. Phys. Commun.* 187, 217–226.
- Howington, S.E., Berger, R.C., Hallberg, J.P., Peters, J.F., Stagg, A.K., Jenkins, E.W., Kelley, C.T., 1999. A model to simulate the interaction between groundwater and surface water. Tech. rep., Engineer Research and Development Center Vicksburg MS.
- Huang, K., Mohanty, B.P., van Genuchten, M.T., 1996. A new convergence criterion for the modified Picard iteration method to solve the variably saturated flow equation. *J. Hydrol.* 178, 69–91.
- Huyakorn, P.S., 2012. Computational methods in subsurface flow. Academic Press.
- Huyakorn, P.S., Springer, E.P., Guvanares, V., Wadsworth, T.D., 1986. A three-dimensional finite-element model for simulating water flow in variably saturated porous media. *Water Resour. Res.* 22 (13), 1790–1808.

- Huyakorn, P.S., Thomas, S.D., Thompson, B.M., 1984. Techniques for making finite elements competitive in modeling flow in variably saturated porous media. *Water Resour. Res.* 20 (8), 1099–1115.
- Jasak, H., 1996. Error analysis and estimation for the finite volume method with applications to fluid flows.
- Jones, J.E., Woodward, C.S., 2001. Newton-krylov-multigrid solvers for large-scale, highly heterogeneous, variably saturated flow problems. *Adv. Water Resour.* 24 (7), 763–774.
- Kirkland, M.R., Hills, R.G., Wierenga, P.J., 1992. Algorithms for solving richards' equation for variably saturated soils. *Water Resour. Res.* 28 (8), 2049–2058.
- Kollet, S.J., Maxwell, R.M., 2006. Integrated surface-groundwater flow modeling: A free-surface overland flow boundary condition in a parallel groundwater flow model. *Adv. Water Resour.* 29 (7), 945–958.
- Kosugi, K., 2008. Comparison of Three Methods for Discretizing the Storage Term of the Richards Equation. *Vadose Zone J.* 7 (3), 957–965.
- Kumar, K., List, F., Pop, I.S., Radu, F.A., 2020. Formal upscaling and numerical validation of unsaturated flow models in fractured porous media. *J. Comput. Phys.* 407, 109138.
- Lai, W., Ogden, F.L., 2015. A mass-conservative finite volume predictor–corrector solution of the 1d Richards' equation. *J. Hydrol.* 523, 119–127.
- Li, Z., Özgen-Xian, I., Maina, F.Z., 2021. A mass-conservative predictor-corrector solution to the 1d Richards equation with adaptive time control. *J. Hydrol.* 592.
- Liu, X., 2013. Parallel Modeling of Three-dimensional Variably Saturated Groundwater Flows with Unstructured Mesh using Open Source Finite Volume Platform OpenFOAM. *Eng. Appl. Comput. Fluid Mech.* 7 (2), 223–238.
- Manzini, G., Ferraris, S., 2004. Mass-conservative finite volume methods on 2-d unstructured grids for the richards' equation. *Adv. Water Resour.* 27 (12), 1199–1215.
- Maxwell, R.M., 2013. A terrain-following grid transform and preconditioner for parallel, large-scale, integrated hydrologic modeling. *Adv. Water Resour.* 53, 109–117.
- Moench, A.F., 1997. Flow to a well of finite diameter in a homogeneous, anisotropic water table aquifer. *Water Resour. Res.* 33 (6), 1397–1407.
- Narasimhan, T.N., Witherspoon, P.A., 1978. Numerical model for saturated-unsaturated flow in deformable porous media: 3. applications. *Water Resour. Res.* 14 (6), 1017–1034.
- Neuman, S.P., 1972. Theory of flow in unconfined aquifers considering delayed response of the water table. *Water Resour. Res.* 8 (4), 1031–1045.
- Neuman, S.P., 1973. Saturated-unsaturated seepage by finite elements. *J. Hydraulics Division* 99 (12), 2233–2250.
- Neuman, S.P., 1974. Effect of partial penetration on flow in unconfined aquifers considering delayed gravity response. *Water Resour. Res.* 10 (2), 303–312.
- Nwankwor, G.I., Gillham, R.W., van der Kamp, G., Akindunni, F.F., 1992. Unsaturated and Saturated Flow in Response to Pumping of an Unconfined Aquifer: Field Evidence of Delayed Drainage. *Groundwater* 30 (5), 690–700.
- Orgogozo, L., 2015. RichardsFoam2: A new version of RichardsFoam devoted to the modelling of the vadose zone. *Comput. Phys. Commun.* 196, 619–620.
- Orgogozo, L., Renon, N., Soulaine, C., Hénon, F., Tomer, S.K., Labat, D., Pokrovsky, O.S., Sekhar, M., Ababou, R., Quintard, M., 2014. An open source massively parallel solver for Richards' equation: Mechanistic modelling of water fluxes at the watershed scale. *Comput. Phys. Commun.* 185, 3358–3371.
- Paniconi, C., Aldama, A.A., Wood, E.F., 1991. Numerical Evaluation of Iterative and Noniterative Methods for the Solution of the Nonlinear Richards Equation. *Water Resour. Res.* 27 (6), 1147–1163.
- Rathfelder, K., Abriola, L.M., 1994. Mass conservative numerical solutions of the head-based Richards' equation. *Water Resour. Res.* 30 (9), 2579–2586.
- Richards, L.A., 1931. Capillary conduction of liquids through porous mediums. *Physics* 1, 318.
- Rubin, J., 1968. Theoretical analysis of two-dimensional, transient flow of water in unsaturated and partly unsaturated soils. *Soil Sci. Soc. Am. J.* 32 (5), 607–615.
- Stehfest, H., 1970. Algorithm 368: Numerical inversion of Laplace transforms [D5]. *Commun. ACM* 13 (1), 47–49.
- Suk, H., Park, E., 2019. Numerical solution of the kirchhoff-transformed richards equation for simulating variably saturated flow in heterogeneous layered porous media. *J. Hydrol.* 579, 124213.
- Tracy, F.T., 2006. Accuracy and performance testing of three-dimensional unsaturated flow finite element groundwater programs on the cray xt3 using analytical solutions. In: 2006 HPCMP Users Group Conference (HPCMP-UGC'06). IEEE, pp. 73–79.
- Trefry, G.M., Muffels, C., 2007. Feflow: A finite-element ground water flow and transport modeling tool. *Groundwater* 45 (5), 525–528.
- van Genuchten, M.T., 1980. A Closed-form Equation for Predicting the Hydraulic Conductivity of Unsaturated Soils. *Soil Sci. Soc. Am. J.* 44 (5), 892–898.
- van Genuchten, M.T., 1982. A comparison of numerical solutions of the one-dimensional unsaturated-saturated flow and mass transport equations. *Adv. Water Resour.* 5 (1), 47–55.
- van Genuchten, M.T., Nielsen, D.R., 1985. On describing and predicting the hydraulic properties of unsaturated soils. *Ann. Geophys.* 3 (5), 615–628.
- Vauclin, M., Khanji, D., Vachaud, G., 1979. Experimental and Numerical Study of a Transient, Two-Dimensional Unsaturated-Saturated Water Table Recharge Problem. *Water Resour. Res.* 15 (5), 1089–1101.
- Šimmek, J., van Genuchten, M.T., Šejna, M., 2008. Development and applications of the hydrus and stanmod software packages and related codes. *Vadose Zone Journal* 7 (2), 587–600.
- Whisler, F.D., Watson, K.K., 1968. One-dimensional gravity drainage of uniform columns of porous materials. *J. Hydrol.* 6 (3), 277–296.
- Williams, G.A., Miller, C.T., 1999. An evaluation of temporally adaptive transformation approaches for solving Richards' equation. *Adv. Water Resour.* 22 (8), 831–840.
- Yeh, G.-T., Shih, D.-S., Cheng, J.-R.C., 2011. An integrated media, integrated processes watershed model. *Computers Fluids* 45 (1), 2–13.
- Yeh, G.T., Ward, D.S., 1980. Femwater: A finite-element model of water flow through saturated-unsaturated porous media. Tech. rep., Oak Ridge National Lab., TN (USA).
- Zyvoloski, G., 2007. Fehm: A control volume finite element code for simulating subsurface multi-phase multi-fluid heat and mass transfer may 18, 2007 laur-07-3359.